Ballistic motion of dust particles in the “Collecting the Big Muley lunar rock” sequence of the Apollo XVI Footage

ABSTRACT

This manuscript develops and integrates the previous study “***Analytical Methods for Tracking Bodies Motions on the Lunar Surface in Apollo XVI Footage***” https://doi.org/10.32388/IA8MXE in order to introduce a robust analytical method to trace and analyze the movement of dust shot during the Apollo XVI mission on the lunar surface. By employing both 2D and 3D analysis techniques, we aim to provide a detailed comparison of the observed kinematic events against theoretical models.

The paper extends a previous work focused on the kinematics of lunar dust utilizing footage from the “Grand Prix” sequence of the Apollo XVI mission "Ballistic motion of dust particles in the Lunar Roving Vehicle dust trails" published in 2012 in the American Journal of Physics by Mihaly Horanyi and Hsiang-Wen Hsu: https://www.researchgate.net/publication/258468670 [Ann. 1 – Ann. 2].

In this further analysis, a sequence in which the astronaut Charles Duke collects an igneous rock (the so-called Big Muley) is tracked. A clearly visible trail of dust is kicked from the left foot of Duke and following a parabolic path, it will reach the lunar ground in the next 25 frames.

By tracking the motion of the dust, we obtain information on its grain size and mechanical behavior in the lunar environment, about the validity of the expected motion models, and - last but not least - about the integrity of the original films in the digital transpositions to which we have access, in particular with respect to the played framerate.

Keywords:

Apollo 16, Lunar dust ballistic motion, Big Muley, Apollo footage

https://doi.org/10.32388/COXHKG.2

SECTION C
Big Muley

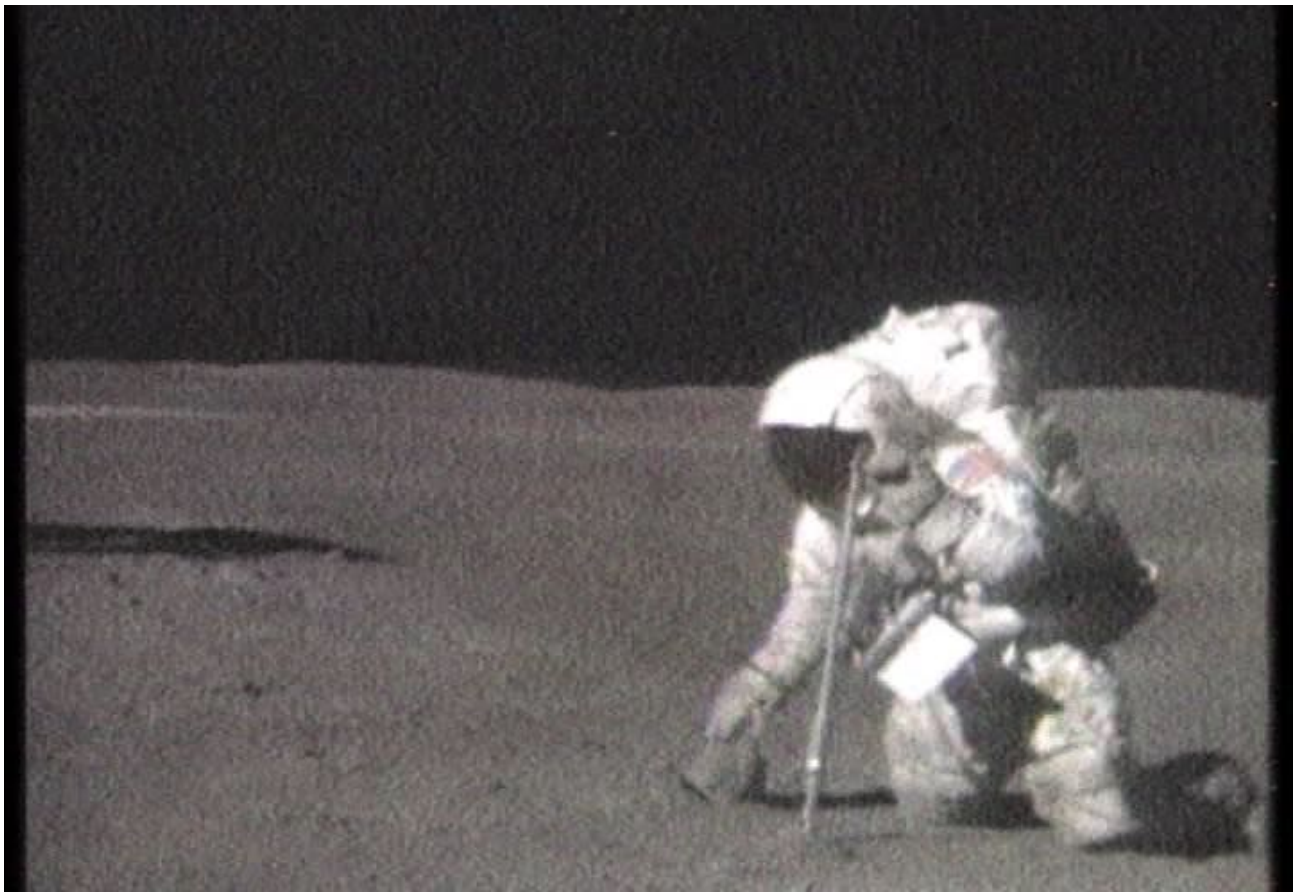

Figure C1 – Charles Duke collects the Big Muley, a frame from the sequence taken by the CTV RCA during Apollo 16

C.1 DESCRIPTION OF THE SEQUENCE [1]:

Houston asks Charlie to collect an 11.729-kilogram, football-sized, anorthosite rock from the rim of Plum Crater. It is the largest rock returned from the moon by any lunar mission and is a coarse-grained, nonvascular, crystalline, igneous rock composed largely of plagioclase. Duke later named it "Big Muley" after Bill Muehlberger, Apollo 16's principal investigator for geology.

C.1.1 Sources: The images used for this study are taken from Apollo 16 Journey to Descartes, complete TV and onboard film © 2005 Spacecraft Film (courtesy NASA). The sequence "Big Muley" is published at this link: https://youtu.be/REoy8eMVKlE

C.1.2 Other official sources containing the same sequence:

- Apollo 16 Lunar Surface Journal Corrected Transcript and Commentary by Eric M. Jones 1997, last revised 16 March 2019. https://www.nasa.gov/wp-content/uploads/static/history/alsj/a16/a16v.1240739.mov
- "Nothing so Hidden" Published by NASA July 12, 2018

---

[1] *https://www.hq.nasa.gov/alsj/a16/a16.sta1.html 124:07:30, Apollo 16 Lunar Surface Journal Corrected Transcript and Commentary by Eric M. Jones 1997. Revised 7 April 2018*

https://plus.nasa.gov/video/apollo-16-nothing-so-hidden-2/

C.1.3 Description of the sequence

Charles Duke approaches the rock, that he is about to gather along the edge of the Plum Crater, in small leaps. The LRV is parked nearby and the RCA TV Camera, mounted on the vehicle for the shooting of EVA 1 activities, films the scene under the remote control of the Mission Control Center in Huston. About 8 meters from the camera, the astronaut makes a final lateral jump from the left to the right of the frame and then reaches the position in which he will bend over to collect the sample. After this leap, the astronaut's right foot approaches the left one, and in rapid succession the left moves away from the camera, advancing slightly to the right of the frame. Both raise a certain amount of dust. A clearly visible trail of dust detaches from the left foot just before it is placed on the ground again, following a parabolic path and reaching the lunar ground in the next 25 frames. Before reaching the ground, the dust spreads opening in a cloud at the end of its motion.

C.2.1 Calculation of the focal length used for shooting.

An image of the reference "set" in which the sequence was shot, comes to our support. In the Apollo 16 Image Library [2], in fact, NASA makes the AS16-109-17800 high-resolution photo available: *https://www.hq.nasa.gov/wp-content/uploads/static/history/alsj/a16/AS16-109-17800HR.jpg*

Figure C2 - Apollo Image Library AS16-109-17800

[2] *https://www.hq.nasa.gov/alsj/a16/images16.html Apollo Image Library, Apollo 16 Figure Captions Copyright © 1996-2017 by Eric M. Jones, last revised 16 March 2019.*

The image was taken with a 60mm lens [3] (therefore not subject to appreciable geometric aberrations). In the centre of the frame, it shows the Rover parked near the Plum Crater and the RCA CTV installed on the vehicle; on the far right there is a rock indicated in the description of the image as Big Muley (Lunar Sample 61016).

Through a perspective analysis performed with the Photoshop CS6 Vanishing Point Filter [4], determining the distance between the lens and Big Muley is elementary. As has already been done in https://doi.org/10.32388/IA8MXE A.2.1.1, once the reference planes that characterize the perspective development of the image have been correctly identified, accurate measurements of the three-dimensional space can be performed. The known dimensions through which it is possible to set up a measuring system can be obtained, once again, from the wheel diameter of the LRV [5] (cm 81.8), which is the reference measurement for height and depth through which we can calibrate the measurement system for the prospective analysis of space.

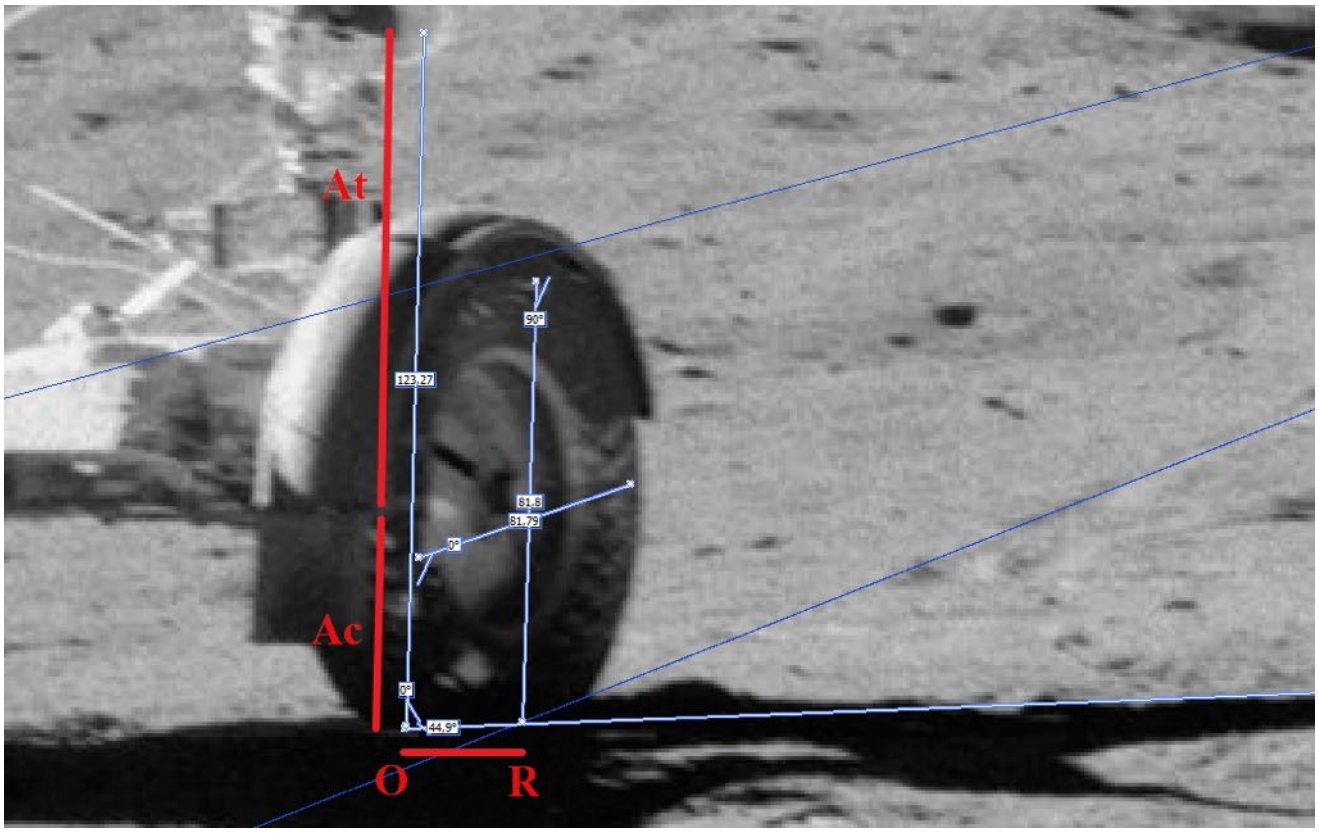

Figure C3 – AIL, AS16-109-17800, calibration of measurement system with Photoshop CS6 Perspective Focus Filter

On the opposite side of the frame, the height that the portion emerging from the lunar soil of the Big Muley rock assumes in the set measurement system (16.4 cm) agrees with the scientific information

[3] *http://pdsimage.wr.usgs.gov/data/a16c-l-mc-2-scanned-images-v1.0/A16MC_0001/DOCUMENT/ap16_data_notes.pdf Apollo 16 Lunar Photography, NASA – National Space Science Data Center, Greenbelt MD 1973 [Ann. 3]*

[4] *https://helpx.adobe.com/uk/photoshop/using/vanishing-point.html Adobe Photoshop User Guide, Image transformations, Vanishing Point Copyright © 2019 Adobe 345 Park Avenue San Jose, CA 95110-2704*

[5] *https://www.nasa.gov/wp-content/uploads/static/history/alsj/LRV_OpsNAS8-25145.pdf Lunar Roving Vehicle Operation Handbook, The Boeing Company LRV Systems Engineering, Huntsville (Alabama), April 19, 1971 [Ann. A6]*

presented in the Lunar Sample Compendium published by NASA [6], thus confirming the correctness of the scale and the perspective plans identified. Below we present in detail the steps performed and the results obtained.

C.2.1.1 Relevant known dimensions.

We fix the lens's projection to the ground as the origin "O" of our system [7], which is placed approximately in correspondence with the internal profile of the vehicle wheel [5].

We indicate with R the ordinate that in our reference system is assumed by the external profile of the wheel, with A_t and A_c respectively the height of the CTV on the chassis [7] and the height of the chassis from the ground in the absence of load [5] (also the thickness of the chassis is considered); finally, with B, the position of Big Muley on the ground.

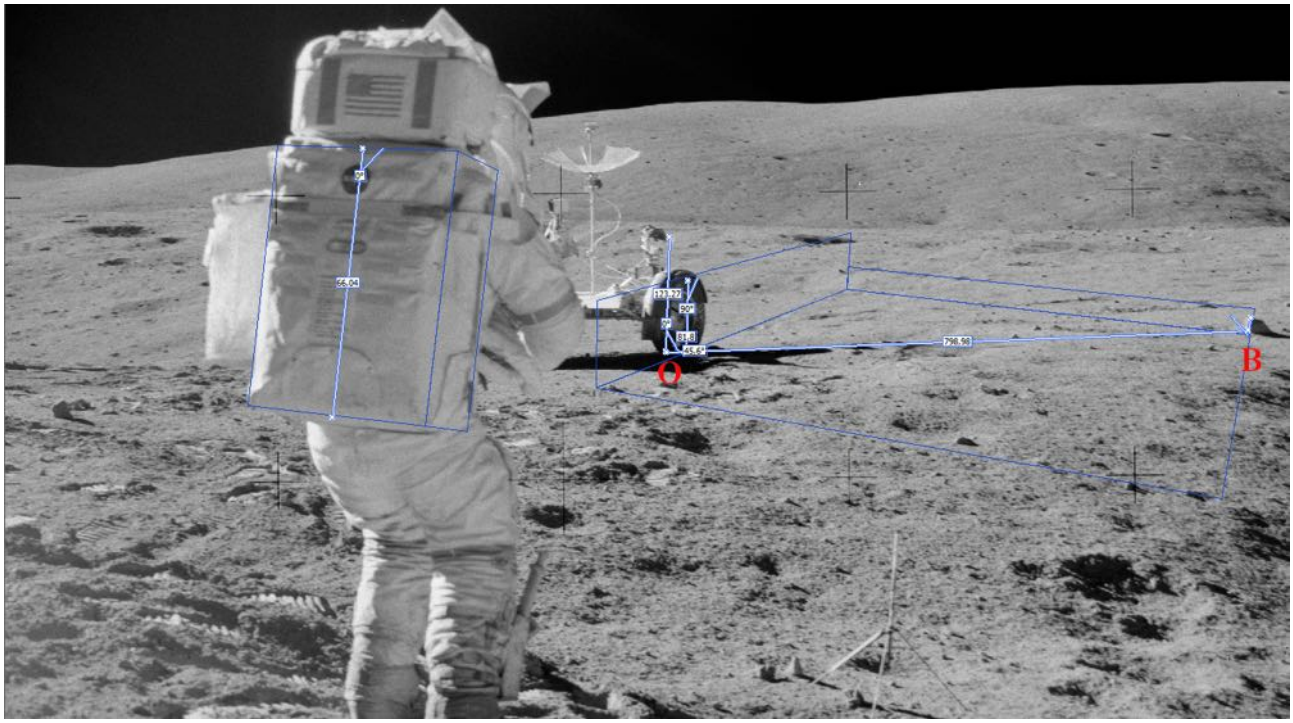

Figure C4 – AIL, AS16-109-17800, Distance of Big Muley from lens

The following measures are known:

Figure C3

- Rover wheel diameter [5]: 81.8 cm (32.2 inches)
- OR = Thickness of wheel [5] = 22.86 cm (9 inches)

The height of the camera on the ground A can be obtained from $A = A_t + A_c$ = 123 cm (48.41 inches)

The experimental error +/- 1.5 px (see C.3.7), on this measure, is calculated as +/- 0.97 cm

---

[6] *https://curator.jsc.nasa.gov/lunar/lsc/61016.pdf 61016 Impact Melt Rock with Shocked/Melted Anorthosite Cap, Lunar Sample Compendium C Meyer 2009 [Ann. C1]*

[7] *https://www.nasa.gov/wp-content/uploads/static/history/alsj/GCTA-Manual.pdf RCA Government and Commercial Systems, Astro-Electronics Division, Princeton NJ 08540; Issued 24 May 1971, Revised January 1972 [Ann. A3]*

Figure C5
- Big Muley above-ground height [6]: 16.4 cm

The position of the cube as a reference for the measurement also indicates the position that the rock had on the lunar soil, allowing us to identify the height of the above-ground portion.

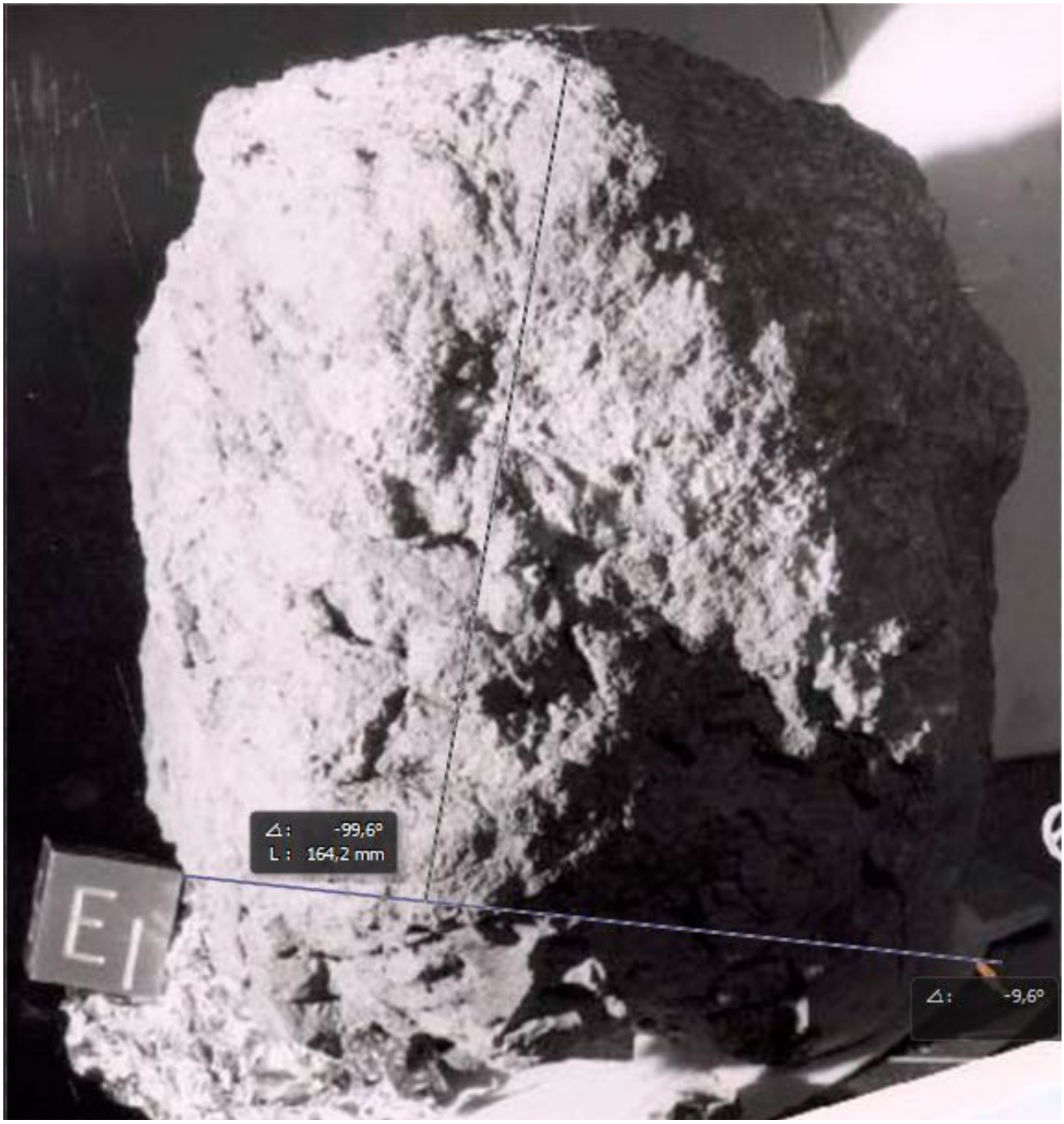

Figure C5 – Dimensions of Big Muley, Lunar Sample Compendium

C.2.1.2 Identification of perspective measurement plans, instrumental error.
The line of contact of the wheel of the LRV with the lunar ground traces the base of the main plane on whose height we will rely on homologous points having the same heights on the circumference of the wheel itself. There is only one vertical plane that allows the measurements of the diameter of

the wheel in width and height concordant. This one, once identified, will allow us to correctly express the perspective. Once the main (vertical) plane, that we will extend up to Big Muley, has been identified, the Photoshop CS6 Vanishing Point Filter allows us to derive orthogonal planes. It will therefore be possible to proceed to derive the horizontal (ground) plane. At this point we derive a second vertical plane from the main plane, extending it to the end of the ground plane to measure the height of the Big Muley from the ground, and we actually obtain confirmation of the correctness of the system: the measure exactly matches the one published on the Lunar Sample Compendium.

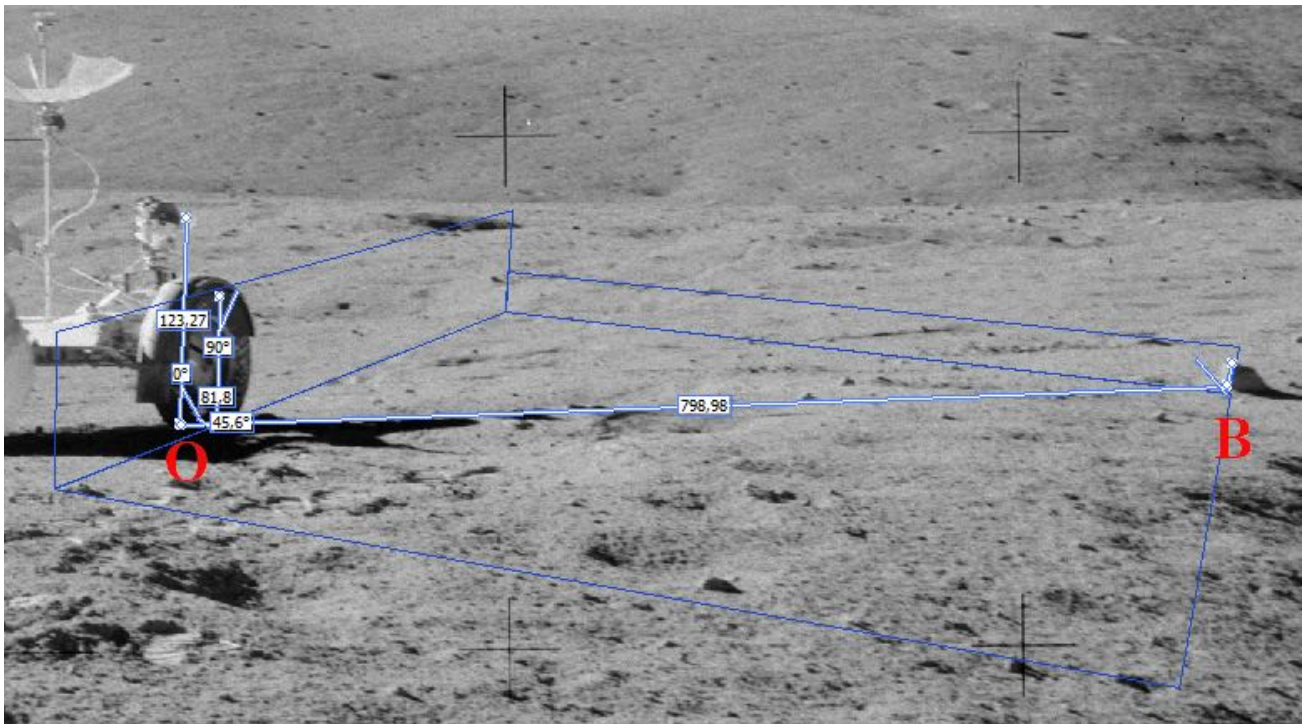

Figure C6 – AIL, AS16-109-17800, results of the measurement

C.2.1.3 Measurement result

Using the metric system just set, the OB distance turns out to be 799 cm. The instrumental error of +/- 1.5 pixels (see C.3.7) on this distance is +/- 1.82 cm. This measurement seems to agree with the available cartography (Figure C7 [8]) [3]

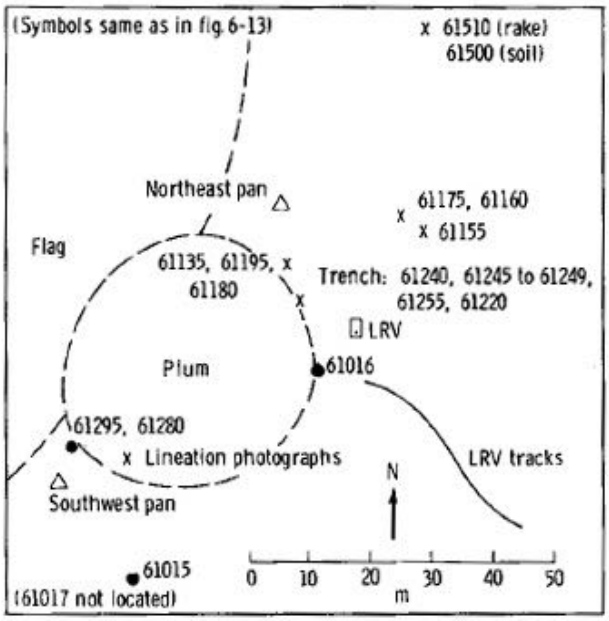

C.2.1.4 Calculation of the distance between the lens and the object

The distance D of the lens from the Big Muley is given by

$$D = \sqrt{(OB^2 + A^2)} = \sqrt{(799^2 + 123^2)} =$$

[8] https://www.nasa.gov/wp-content/uploads/static/history/alsj/a16/a16psrf6-21.jpg
Apollo 16 Preliminary Science Report, NASA Manned Spacecraft Center, Scientific & Technical Information Office 1972

= 808 cm (+/- 1.95 cm)

C.2.1.5 Conclusions on the calculation of the foca *Figure C7 - Planimetry of Station 1, Eva 1, Apollo 16*

Indicated as BM_t the height of Big Muley on the CTV sensor, and BM_l as the height of the rock on the lunar ground, the focal used F is given by the relationship

$$F = D \cdot \frac{BM_t}{BM_1}$$

By opening one of the images of the sequence being studied, and setting the sensor dimensions [7] (12.8 x 9.6 mm) as reference dimensions we can find BM_t = 0.6 mm with an instrumental error of 1 pixel equivalent to +/- 0.05 mm

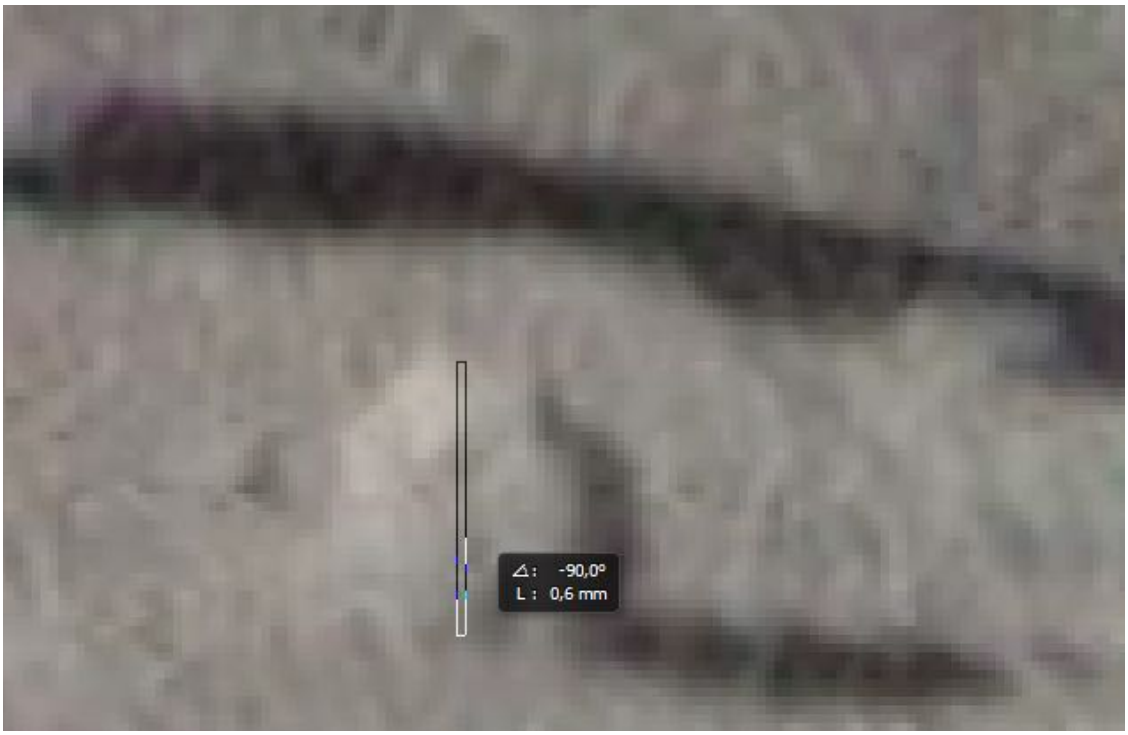

Figure C8 – Enlargement of Big Muley in the sequence taken from CTV RCA Camera

Therefore, we obtain: F = $F = 8080 \cdot \frac{0,6}{164}$ = 29.56 mm (+/- 2.53 mm)

To evaluate the percentage of distortion to be applied based on the focal length used, it is necessary to express the latter in terms of "equivalent focal length" Fe, comparing it to a standard sensor (36mm X 24mm full-frame, 35mm) instead of the sensor of 16 mm with which the scene was shot. If D is the diagonal of the 16 mm sensor and Ds is the diagonal of the standard format (43.3 mm), then:

$$Fe = F \cdot \frac{D_S}{D} = 29.56 \cdot \frac{43,3}{16} = 80 \text{ mm (+/- 6.8 mm)}$$

C.2.2 Conclusions on the geometric aberration of the images

Since the typical distortion of CTV was estimated at 2% due to its spherical photocathode, and the equivalent focal length used for the sequence can be identified between 73 and 87 mm (light telephoto), it is appropriate to consider a percentage of distortion higher than 2% and less than 3% (maximum declared). The choice of the 2,5% value, as a percentage of positive distortion (pincushion) to be corrected on the images of the sequence, was confirmed as the most accurate for the exact correspondence of the known dimensions within the measurement system that was built to obtain the spatial values of the sequence under study. The correction was made through the Photoshop CS6 Lens Correction filter [9].

C.3.1 Launch dynamics

With reference to the events already described in https://doi.org/10.32388/IA8MXE paragraph C.1.3, we analyse the elements and forces that make up the system filmed by CTV in the sequence of about 2 seconds that originates from the second 0:30 of the video already indicated, available at the address https://youtu.be/REoy8eMVKlE. There are two different motions of lunar dust raised respectively by the right foot and the left foot of the astronaut Charles Duke. The first trail of dust raised by the right foot in rapid approach to the left originates in the first frames of the sequence.

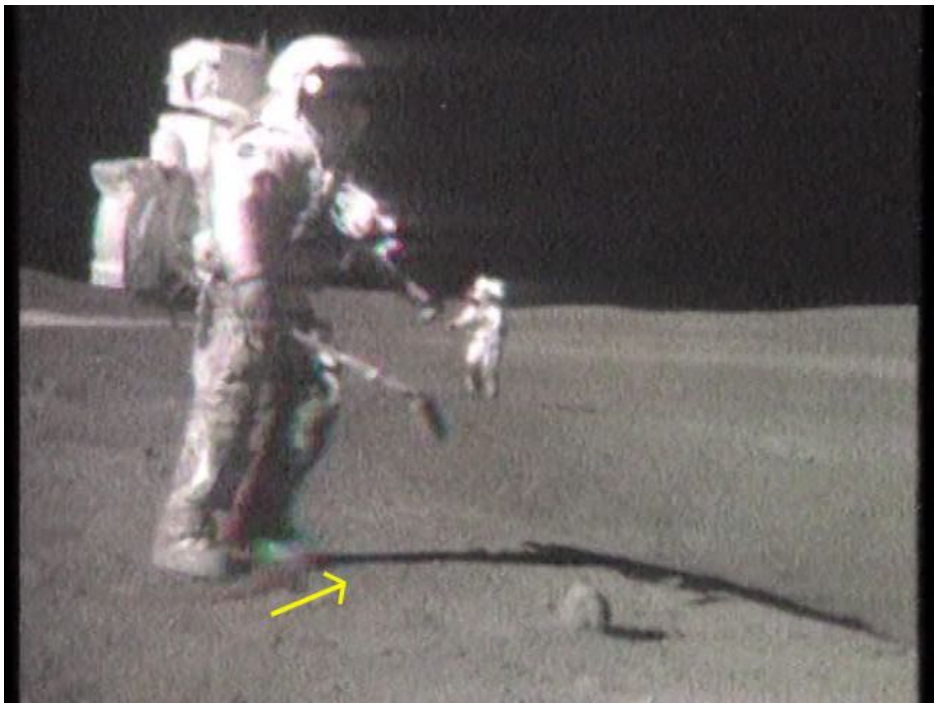

Figure C9 – Direction of first dust launch (right foot)

[9] *https://helpx.adobe.com/photoshop/using/correcting-image-distortion-noise.html Adobe Photoshop User Guide, Image repair and restoration, Correct image distortion © 2019 Adobe 345 Park Avenue S. Jose, CA 95110-2704*

As soon as the left foot detaches itself from the ground, a second trail of dust, more evident, departs from Duke's boot in the direction of the Big Muley, falling back on the ground after about 20 frames: we will deal with this second trail. The direction of the second cloud of regolith can be determined thanks to its shadow cast on the lunar ground, which advances precisely towards the rock subject of the interest of the astronauts, moving away from Duke's shadow at an angle of about 5°. It was not possible to determine if this more persistent trail was lifted off from the ground by the astronaut's left foot, if the dust had already been deposited on the boot before launching, or if the same foot involuntarily kicked the dust raised by the right foot, diverting it from its original trajectory.

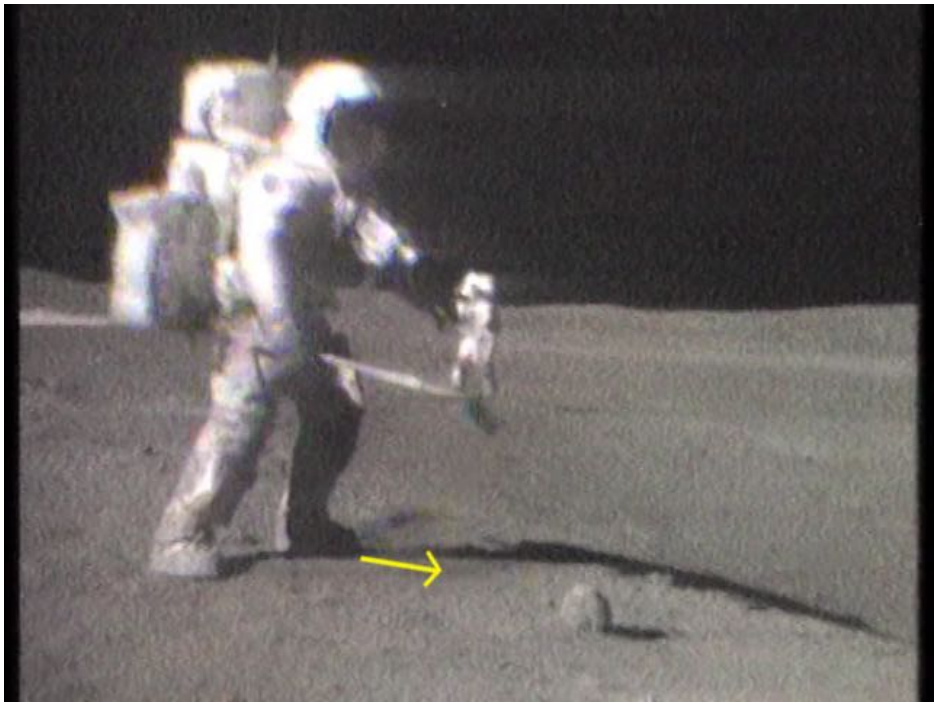

Figure C10 – Direction of examined dust launch

C.3.2 Analysed frames

In the annex n° C2 [*Ann. C2*] there are the frames that refer to the motion studied, extracted from the video in uncompressed format. Among them, an interval of 20 frames was chosen, in which the position of the head of the dust train was evident. The most advanced point of this trail has been traced regardless of the chaotic shape that the cloud gradually assumed in its progression, similar to what was proposed by the authors of the study "Ballistic motion of dust particles in the Lunar Roving Vehicle dust trails" cited in the introduction. In fact, Mihaly Horanyi and Hsiang-Wen Hsu affirm: "*For a tenuous dust cloud, where the inter-particle collisions are rare, a dust particle follows a ballistic path from its ejection until it returns to the surface*". The apical region of the cloud actually presents conditions that allow the model to be reduced to an independent material point, that is to a single ballistic particle. This choice was also made necessary in consideration of the particular production process suffered by the images, especially in relation to what is described in https://doi.org/10.32388/IA8MXE paragraph A.3.2. Only the most advanced part of the moving cloud can guarantee full compliance with the timeline, given that each frame consists of the superposition of 4 half-fields photographed within 1/15 of a second.

The cloud, in the descending part of its parable, denotes a progressive rarefaction, tending to fan out. The measurements continued to trace its most evident part, keeping the direction indicated by the shadow cast on the ground, a direction that is evidently followed by most of the material thrown.

C.3.3 Measurement system set up [*Ann. C3*]

As in the case of determining the focal length used for shooting (see C.2.1), the Photoshop CS6 Vanishing Point Filter was used for the measurements [10]. To do this, the frames were exactly superimposed in a multilevel project, which is very simple since we are in the presence of a sequence shot by a fixed camera. Then we proceeded to define the measurement system, through perspective analysis, first in 2D (monoscopic photogrammetry) [11] and then in 3D. Starting from frame 6 of the sequence, the Vertical Axis and the Ground Line have been identified.

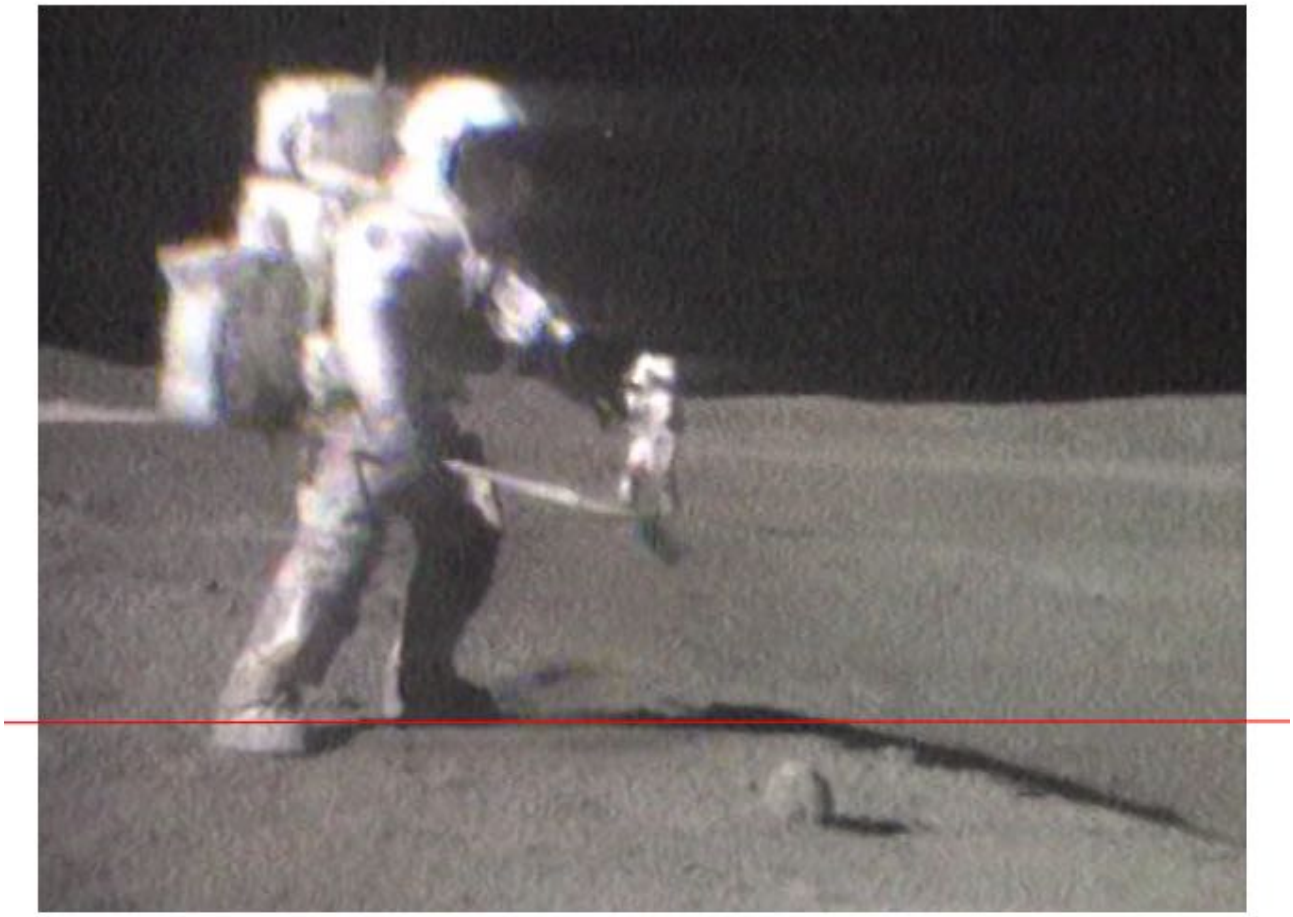

Figure C11 – Ground Line

[10] https://helpx.adobe.com/uk/photoshop/using/vanishing-point.html *Adobe Photoshop User Guide, Image transformations, Vanishing Point Copyright © 2019 Adobe 345 Park Avenue San Jose, CA 95110-2704*

[11] https://onlinelibrary.wiley.com/doi/pdf/10.1111/j.1477-9730.2005.00343_1.x *Manual of Photogrammetry, American Society of Photogrammetry (Washington D.C.) and Remote Sensing (Bethesda Maryland), Fifth Edition 2004.*

Considering that the camera is stably positioned on the same ground plane on which astronaut Charles Duke walks (as confirmed by Fig C6), it is possible to choose as reference system axes orthogonal to the plane of view. The ground line GL is suitably placed at the base of the astronaut's left boot and is extended so that it coincides with the flat part of the projection of his shadow. The first position detected by the tracked dust spurt head is chosen as the system origin.

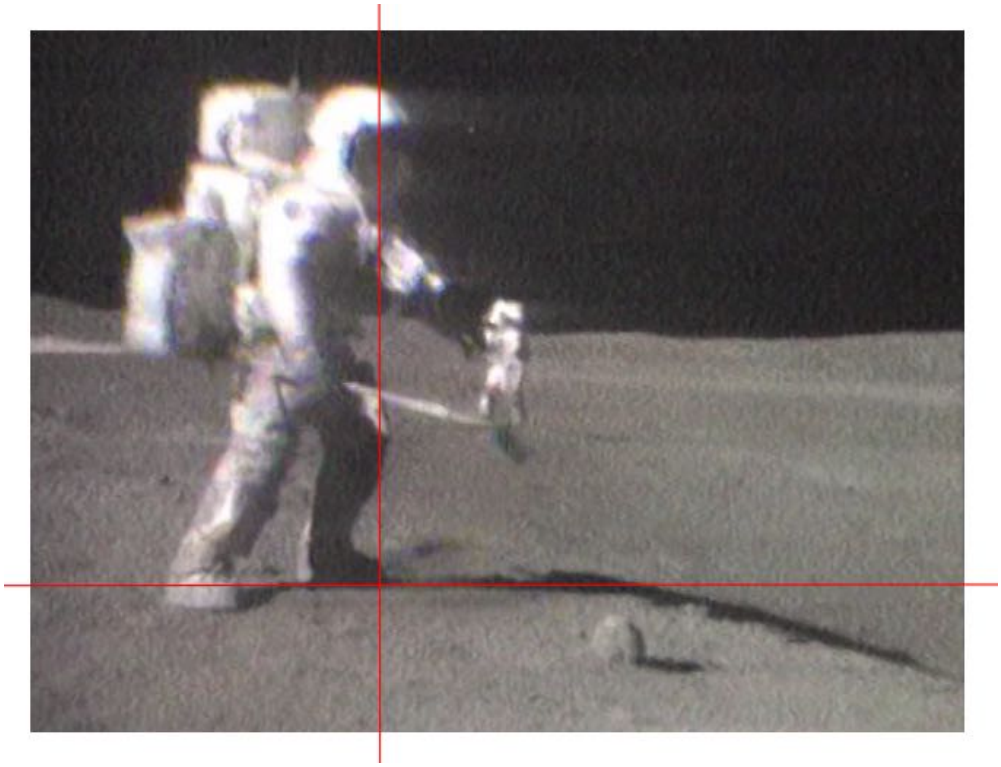

Figure C12 – Z axis orthogonal to the ground line GL

Finally, using frame 8 of the sequence, in which the apex of the shadow of the dust spurt is particularly evident, this point has been joined with the origin of the axes, identifying the trajectory of the motion of the dust in its projection on the lunar ground and thus obtaining the X axis.

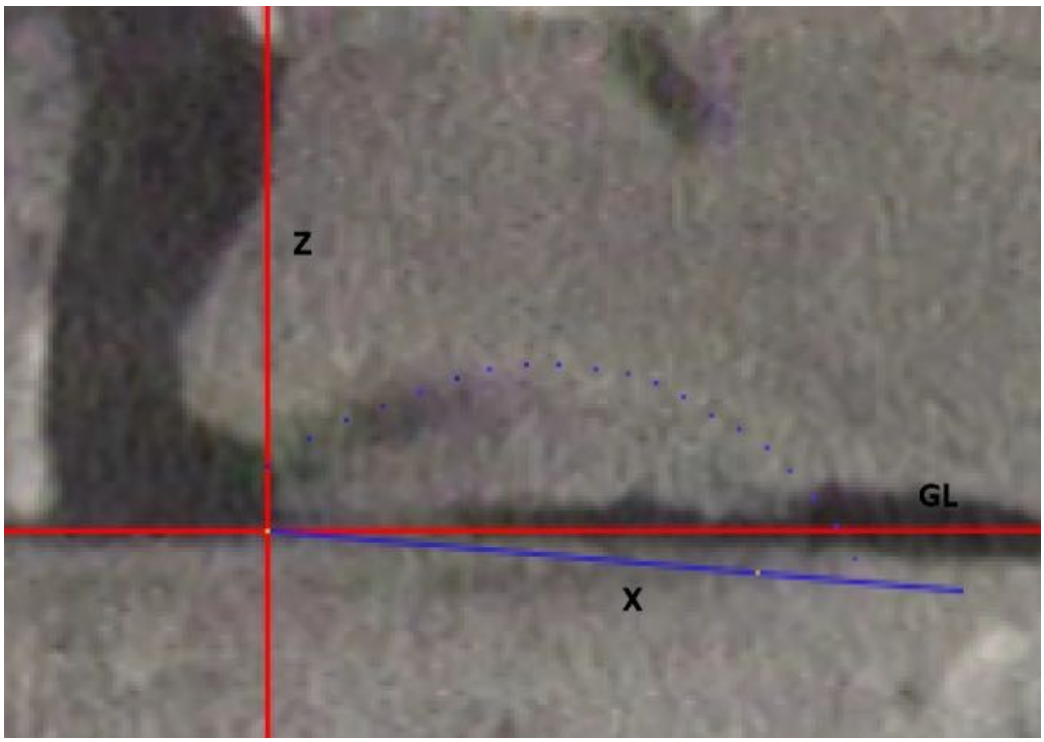

Figure C13 – Tracking of motion in space

At this point, from 2D analysis, we have moved to 3D analysis using the Photoshop CS6 Vanishing Point Filter. Starting from the lines identified in frame 6, the perspective planes necessary to define the 3D measurement system were defined. Plane A coincides with the plane of view. Plan B forms an angle of about 22 degrees with the latter and identifies the position of Duke's left foot (it will be used for system calibration). The C plane identifies the path followed by the dust and is inclined by a further 6 degrees (28 ° in total with respect to the plane of view).

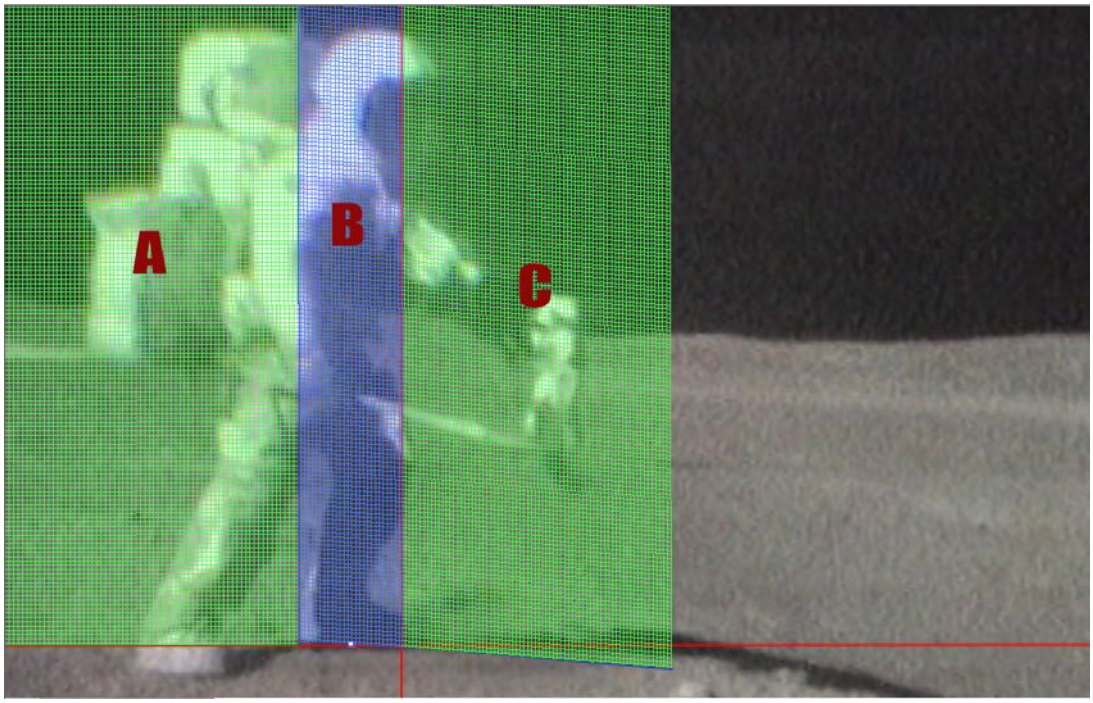

Figure C14 – Measurement planes

The measurements of the dust spurt head tracking are carried out on the C plane identifying the vertical and horizontal coordinates by positioning perfectly orthogonal segments on the same plane.

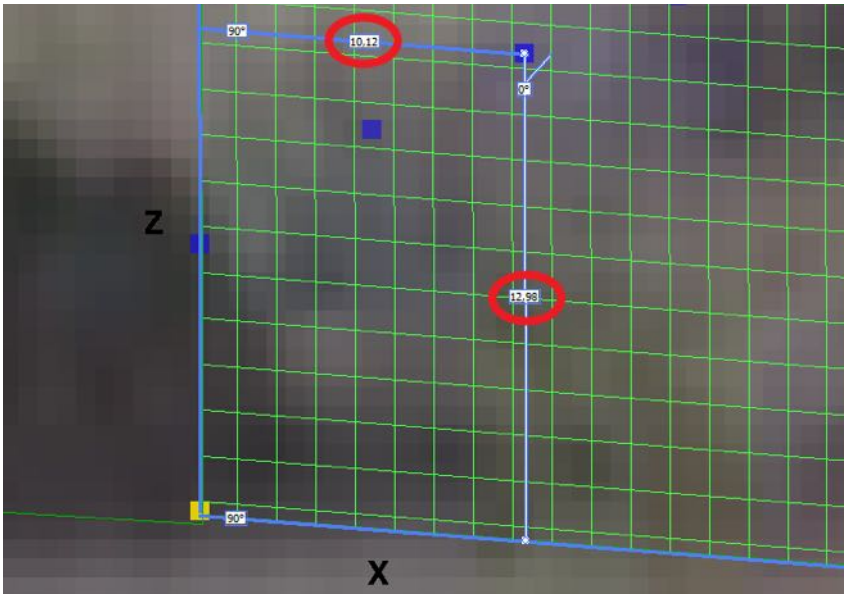

Figure C15 – Example of measurement, frame 2

C.3.4 Configuration of the perspective scale starting from known measures.

The planes shown in Figure C14 are connected in a single system, and thus they maintain correct proportions. It is necessary to introduce at least one known measure to define the scale. In this regard, we use the technical data of the astronaut equipment already identified in https://doi.org/10.32388/IA8MXE A.2.1.1.1: the Training PLSS Unity worn by Charles Duke (height 66.04 cm, top thickness 22.22 cm) [12]. Following the appropriate corrections of the display aspect ratio and pixel aspect ratio (see https://doi.org/10.32388/IA8MXE A.3.4.1 and A.3.4.2), and the identification of the right measurement plans, the first confirmation that the system set up is correct with respect to the real proportions is implicit in the fact that these two known measures are compatible with the detectable ones on the examined images (see Figure C16).

Further confirmations, about the correctness of the system in the proportions and interpretation of the perspective, come from two other elements in the image of which we can find the real size. The first is the length of the boot worn by Charles Duke. The production measures of the Moon Boot were two: Omed (336 mm long) and Olge (368 mm long). The smaller size corresponds exactly to the one we can check in the image (see Figure C18) [13].

---

[12] *Measurements of Apollo 16 Training Unit, Courtesy Dean Eppler, NASA, Lyndon B. Johnson Space Center, Houston Texas, USA. The PLSS Unity measurements do not include the OPS module placed above.*

[13] *https://issuu.com/moonandspace/docs/moon_boot The story of the Apollo lunar overshoe and the race to walk on the moon, © David H. Mather 2014 – Published by Space Effects Limited (Durley UK)*

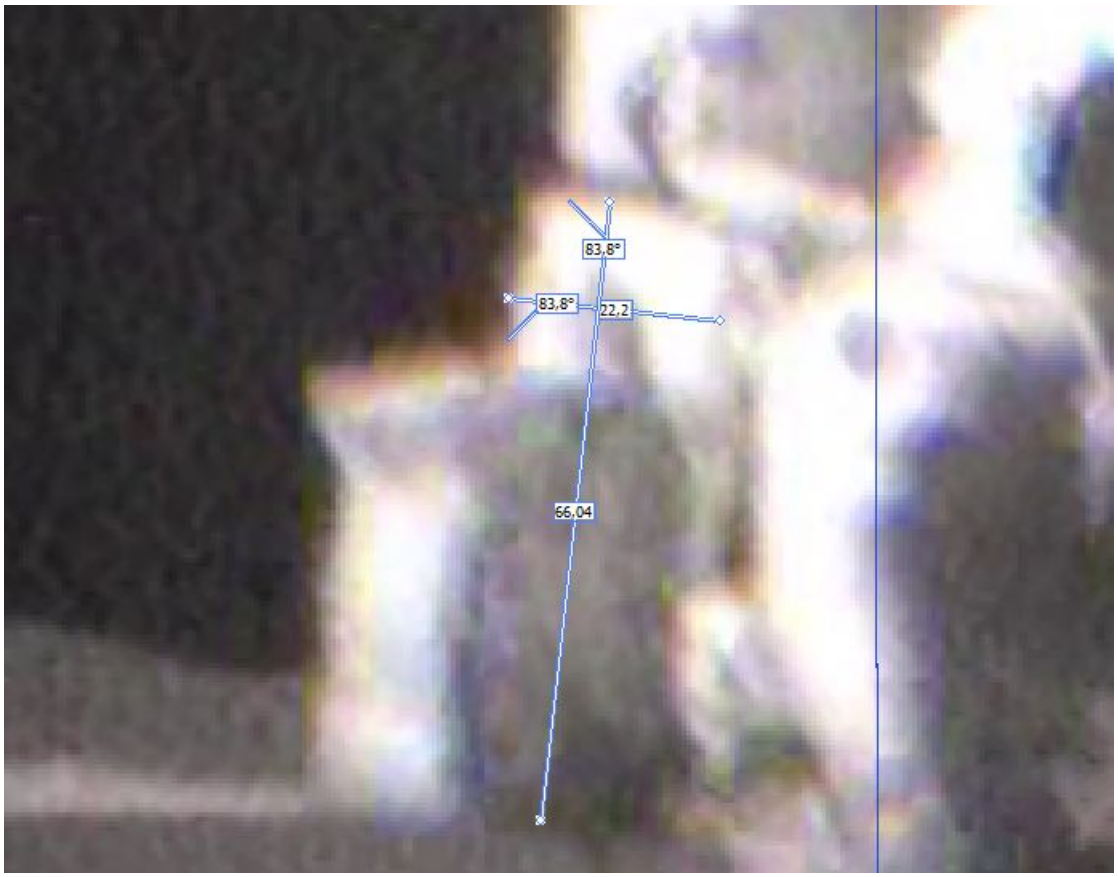

Figure C16 – Apollo 16, dimensions of the Training PLSS unity in the images of the examined sequence

Boot sizes

The moon boot was produced in two sizes – OMED and OLGE, and the difference can be seen in the number of ribs on the sole of the boot - there are eight on the OMED and nine on the OLGE.

The soles measure 13¼" (336mm) x 6" (52mm) for the smaller size and 14½" (368mm) x 6½" (165mm) for the larger size.

Astronauts that wore a street shoe of size 11(US) or larger would use the OLGE size. For example, Jim Lovell of Apollo 13 wore a size 11(US) shoe, whilst Neil Armstrong's shoe size was 9½(US).

Figure C17 – The production measures of the Moon Boots

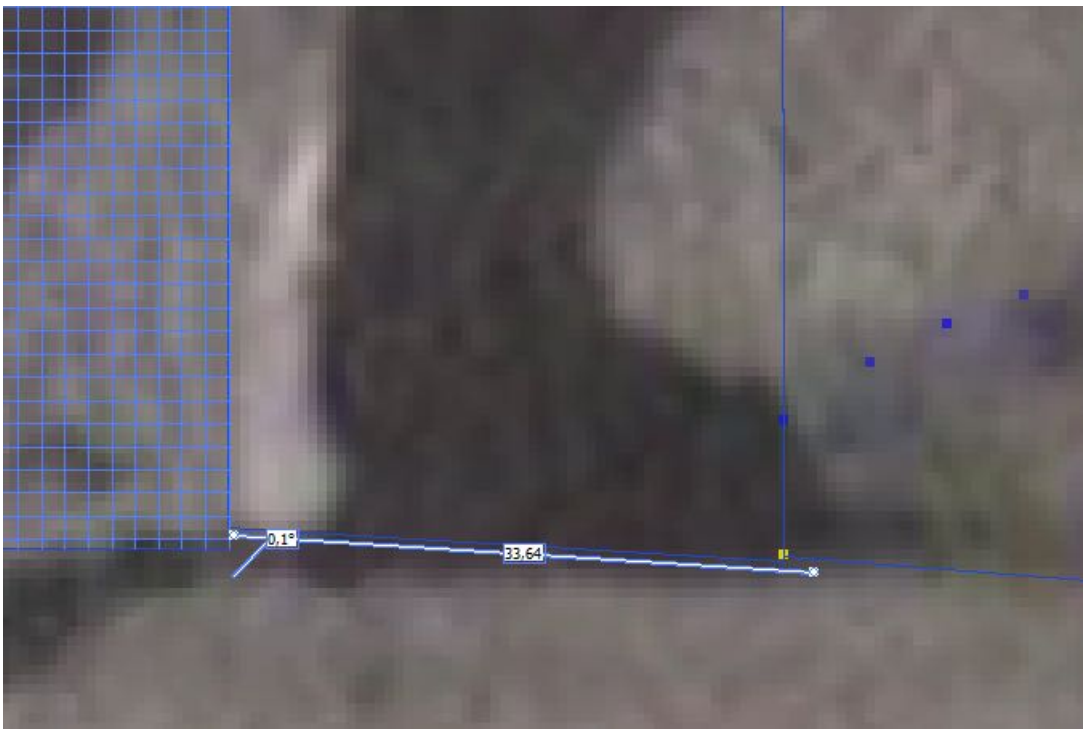

Figure C18 – Measurement of the left Moon Boot of Charles Duke in the examined sequence

The second element is the height above the ground of the Big Muley: 16,4 cm (see Figure C5), which is confirmed with excellent approximation by the relief on the CTV image.

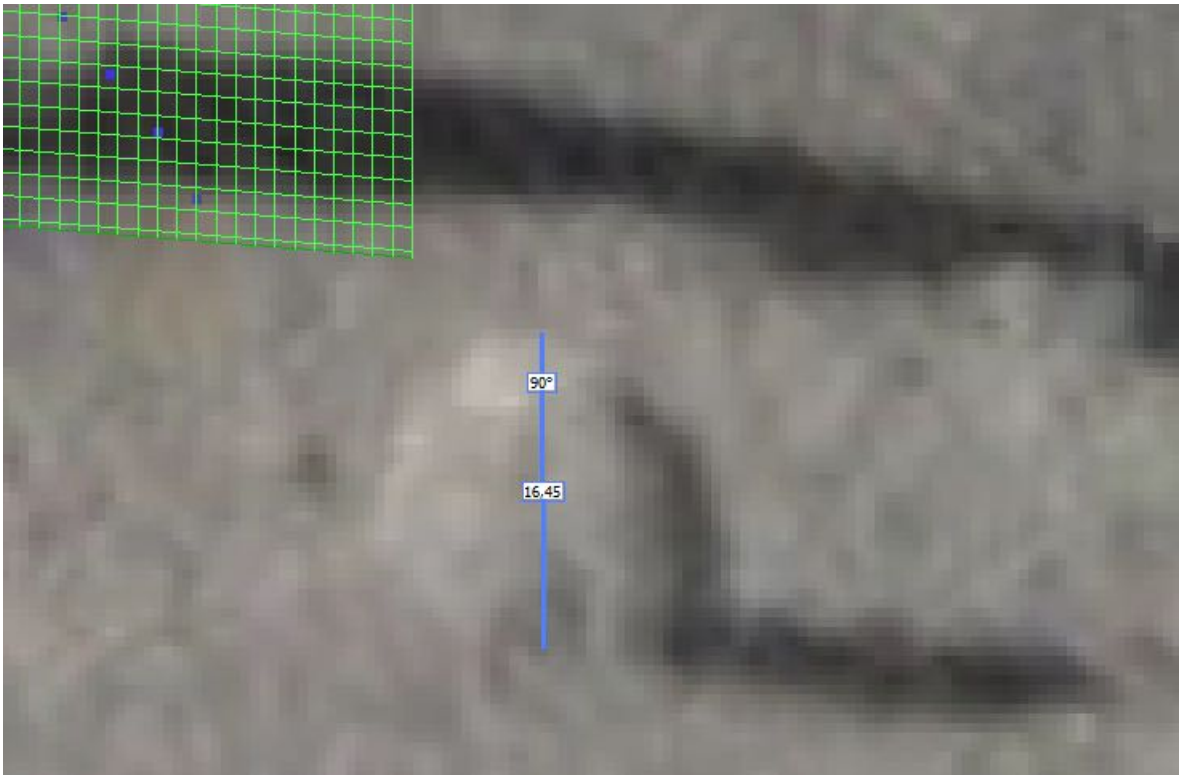

Figure C19 – Height above the ground of the Big Muley

C.3.5 Finding the position of the material point in the frames of the sequence.

With reference to what has already been described in C.3.1 about the dynamics of the launch and the reasons that led to the measurement of the most advanced part of the cloud of dust launched by the boot of the astronaut Charles Duke in the analysed sequence, we present the graphic elaborations collected in Annex n° 32-33 [*Ann. C4* – *Ann. C5*] which describe how the head of the aforementioned cloud, reduced to a material point, was identified frame by frame.

The identification took place without the use of particular filters, so as not to condition the result with artefacts and noise reduction processes that could reduce or alter the information available within the images. Before positioning the point, whose coordinates were subsequently collected thanks to the measurement system implemented, particular lines, able to describe the most advanced front of the spurt, were identified with the Photoshop CS6 "Magnetic Lasso" automatic selection tool.

In some cases, when evident, the positioning of the point did not present any particular problem. For example, the positions of the cloud head recorded at frame 0 and frame 19 are very evident, so much that these frames have been adopted as the beginning and end of the sequence.

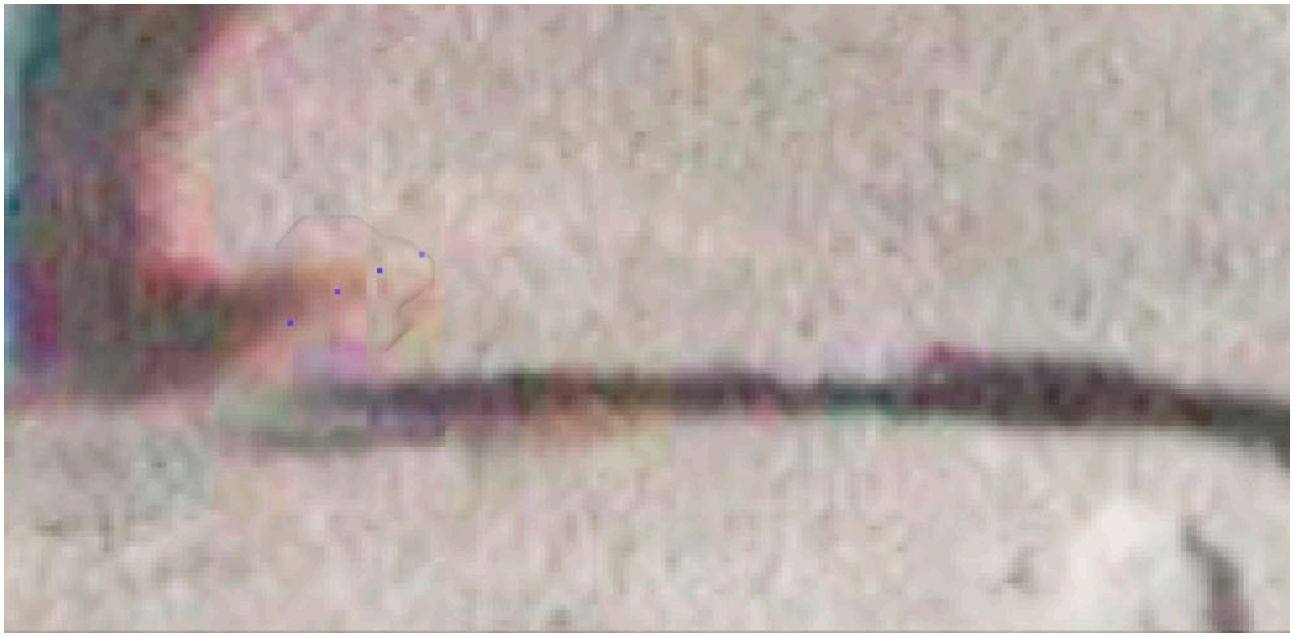

Figure C20 – Graphic elaboration for identifying the head of the dust trail: frame 3/20

Some frames do not allow a sufficiently certain identification of the dust trail tip, so they were left out in the final tracking. These are the frames: 10-11-13-14-15-17-19. Frame 0 does not seem to correspond with the instant of the launch: probably the launch point can be identified in the two previous frames, even if the detection is difficult given the interpretative difficulties that these images present (probably due to the superposition of the two spurts of dust kicked by the Astronaut, first with the right foot and then with the left one).

The darker area of the cloud does not necessarily represent the most densely populated with particles and therefore more compact and advanced. Due to the superposition of the sequential fields recorded by the CTV camera within the analysed frames, it most likely corresponds to the position of the trail of dust resumed in the intermediate fields forming the single frame, which appeared in it twice (see https://doi.org/10.32388/IA8MXE A.3.2).

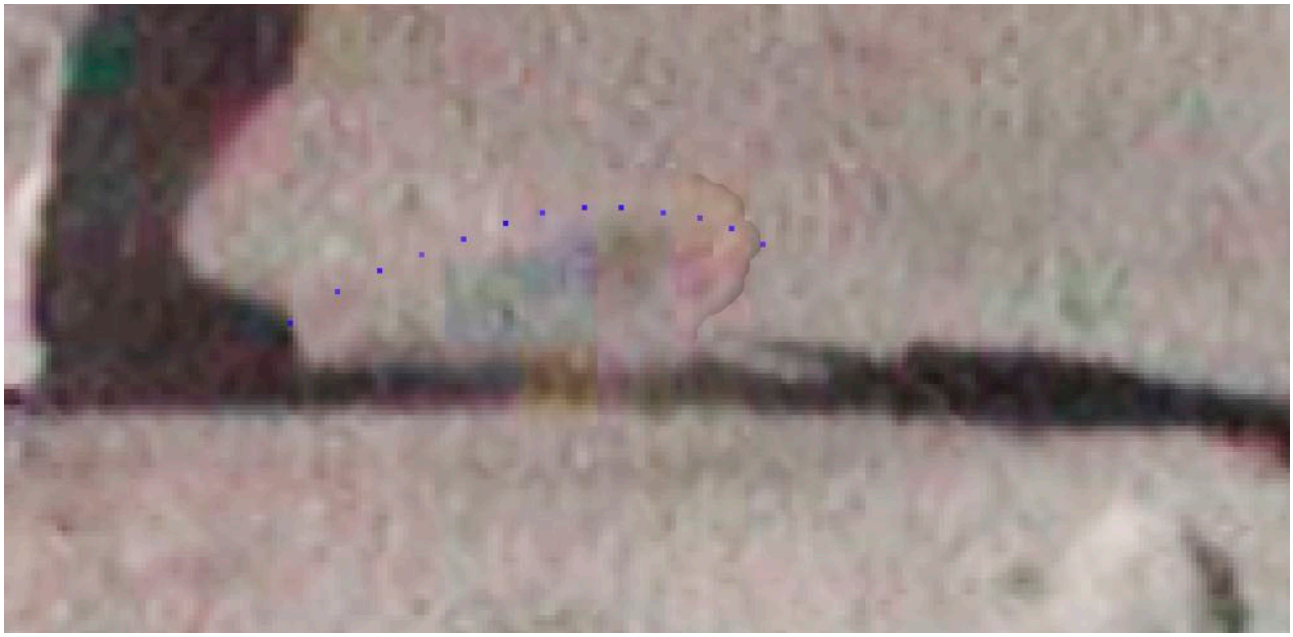

Figure C21 – Graphic elaboration for identifying the head of dust trail: frame 12/20

An animation that exemplifies the motion of the material point at 1fps is available at https://youtu.be/tOg70CDvzbE [*Ann. C6*]

C.3.6 Measurements [*Ann. C7*]

Table C1 on the right displays the measurements obtained in relation to the 20 frames of the sequence. We refer to Annex C8 for the consultation of the screenshots that document the measurements made. [*Ann. C8*]

Frame	Time (s)	X (m)	Z (m)
0	0,000	0	0,071
1	0,033	0,053	0,106
2	0,067	0,101	0,13
3	0,100	0,148	0,148
4	0,133	0,195	0,166
5	0,167	0,243	0,185
6	0,200	0,285	0,199
7	0,234	0,333	0,207
8	0,267	0,374	0,209
9	0,300	0,422	0,208
10	0,334	0,463	0,205
11	0,367	0,5	0,198
12	0,400	0,535	0,185
13	0,434	0,571	0,167
14	0,467	0,607	0,154
15	0,501	0,643	0,136
16	0,534	0,673	0,113
17	0,567	0,702	0,084
18	0,601	0,732	0,055
19	0,634	0,756	0,022

Tab. C1 – Big Muley: metric data collected

C.3.7 Experimental Error and its propagation

The measurements taken were expressed by the Photoshop CS6 Vanishing Point Filter directly on the real scale. The accuracy of the identified values, however, depends both on the calibration of the scale, carried out by associating the known dimensional value (see C.3.4) to a detected segment, and on the individual measurements. In both cases, the sensitivity of the instrument (which we will call u) is equal to 1 pixel equivalent to 0,005 m in reality:

u = +/- 0.5 px = +/- $2.5*10^{-3}$ m.

C.3.7.1 Evaluation of the calibration error.

Therefore, the calibration by identifying known measurements requires us to consider a first experimental error equal to the minimum division of the system. Each dimension, enhanced and broken down into its Cartesian components, identifies the scale of the measurement plane on which it resides. Being orthogonal planes, they collectively contribute to defining the measurement system as a whole. The software used, therefore, associates to each point of the plane a pair of coordinates P(x, y) so that the distance between two points will be expressed by the relationship:

$f(x, y) = P_2(x_2, y_2) - P_1(x_1, y_1) = \sqrt{(x_2 - x_1)^2 + (y_2 - y_1)^2}$

in which the components x and y obtained from the difference between $x_2 - x_1$ and between $y_2 - y_1$ are affected with an error $2u$ = +/- 1 px = +/- $5*10^{-3}$ m. The distance between points that reside on different planes (provided these planes are orthogonal to each other) can be expressed by a similar relationship. The uncertainty on the distance calculated by the software can be determined starting from the uncertainties of each variable, by calculating the partial derivatives of the function f with respect to them:

$\Delta f = \Delta f(\Delta x, \Delta y) = 2u * \sqrt{(\frac{\partial f}{\partial x})^2 + (\frac{\partial f}{\partial y})^2}$

With u = 1, the distance can be expressed as follows:

$D_1 = (\frac{\partial(\sqrt{x^2+y^2})}{\partial x})^2 = \frac{x^2}{x^2+y^2}$ $\qquad$ $D_2 = (\frac{\partial(\sqrt{x^2+y^2})}{\partial y})^2 = \frac{y^2}{x^2+y^2}$

Therefore, the distance will be $D = \sqrt{x^2 + y^2}$ with uncertainty $2u = 1$. This demonstrates that, given an identical initial uncertainty on the coordinates of two points, the uncertainty of their distance maintains the same value.

C.3.7.2 Evaluation of the error in the measurement.

At this point, we want to identify the position of the material point on the measurement plane. We must therefore consider again the error u due to the minimum division of the instrument. The experimental error of each measurement can therefore be quantified in

$3u$ = +/- 1.5 px = +/- $7.5*10^{-3}$ m.

In order to express the maximum error which burdens each measurement, the module of experimental error will be composed with the module of accuracy error, through the quadrature sum method: $ErrMax = \pm \frac{\sqrt{(u^2 + Err^2)}}{2}$

C.3.8 Discussion of results

The analysis of the results in order to identify the best fit of the expressed parabolic curve is carried out with the professional software Origin Pro 2018 [*Ann. C9*]. The equations of motion represented by the model described above are the following:

E1) $X_{mod}(t) = X_0 + (V_{X_0} \cdot t)$

E2) $Z_{mod}(t) = Z_0 + (V_{Z_0} \cdot t) - (\frac{1}{2} \cdot g \cdot t^2)$

E3) $X_{ErrMax} = \pm \frac{\sqrt{u^2 + (X_x - X_{x+1})^2}}{2}$ $\qquad$ E4) $Z_{ErrMax} = \pm \frac{\sqrt{u^2 + (Z_x - Z_{x+1})^2}}{2}$

Equation: X = Intercept + Slope · t

Equation	y = a + b*x
Report Status	New Analysis Report
Weight	Instrumental
Special Input Handling	
Data Filter	No

Input Data

Masked Data - Values Excluded from Computations

Bad Data (missing values) -- Values that are invalid and thus not used in computations

Parameters

		Value	Standard Error	t-Value	Prob>|t|
x	Intercept	0,03479	0,00981	3,54531	0,00403
	Slope	1,19835	0,02687	44,59834	1,04361E-14

Slope is significantly different from zero (See ANOVA Table).
Standard Error was scaled with square root of reduced Chi-Sqr.
Some input data points are missing.

Statistics

	x
Number of Points	14
Degrees of Freedom	12
Residual Sum of Squares	5,89134
Pearson's r	0,997
R-Square (COD)	0,994
Adj. R-Square	0,9935

Summary

	Intercept		Slope		Statistics
	Value	Standard Error	Value	Standard Error	Adj. R-Square
x	0,03479	0,00981	1,19835	0,02687	0,9935

ANOVA

		DF	Sum of Squares	Mean Square	F Value	Prob>F
x	Model	1	976,49463	976,49463	1989,01191	1,05471E-14
	Error	12	5,89134	0,49094		
	Total	13	982,38597			

At the 0.05 level, the slope is significantly different from zero.

Equation: Z = Intercept + B1 · t + B2 · t^2

Equation	y = Intercept + B1*x^1 + B2*x^2
Report Status	New Analysis Report
Weight	Instrumental
Special Input Handling	
Data Filter	No

Input Data

Masked Data - Values Excluded from Computations

Bad Data (missing values) -- Values that are invalid and thus not used in computations

Parameters

		Value	Standard Error	t-Value	Prob>|t|
z	Intercept	0,07407	0,00256	28,89181	1,00382E-11
	B1	0,93393	0,01854	50,36791	2,33147E-14
	B2	-1,62066	0,02995	-54,10735	1,06581E-14

Standard Error was scaled with square root of reduced Chi-Sqr.
Some input data points are missing.

Statistics

	z
Number of Points	14
Degrees of Freedom	11
Residual Sum of Squares	0,77657
R-Square (COD)	0,99628
Adj. R-Square	0,99561

Summary

	Intercept		B1		B2		Statistics
	Value	Standard Error	Value	Standard Error	Value	Standard Error	Adj. R-Square
z	0,07407	0,00256	0,93393	0,01854	-1,62066	0,02995	0,99561

ANOVA

		DF	Sum of Squares	Mean Square	F Value	Prob>F
z	Model	2	208,05863	104,02931	1473,5593	4,34097E-14
	Error	11	0,77657	0,0706		
	Total	13	208,8352			

At the 0.05 level, the fitting function is significantly better than the function y=constant.

Figure C22 – Fit of the motion curve with Origin Pro: parameters obtained on the two axes

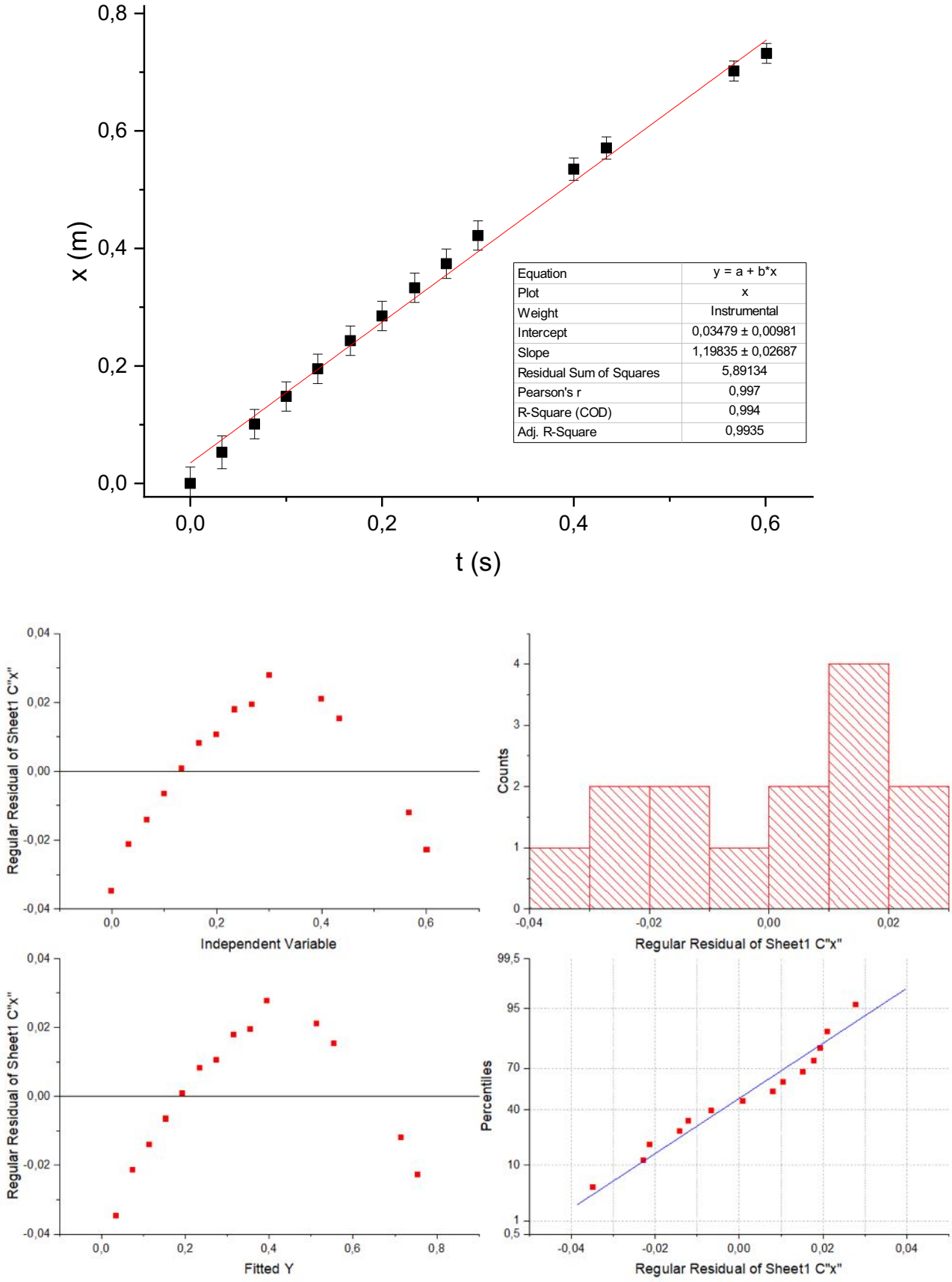

Figure C23 – X-axis fit with maximum error range and data variability analysis (Origin Pro)

As regards the X axis the fit software proposes a horizontal speed of the dust trail of approximately 1.20 m/s, but the problem is that the data collected only partially validates the linear model.

The best estimation of Z-axis gravity acceleration in the tracked sequence is g_{or} = *-3.24 ± 0.060* m/s^2 (Standard Err). A value significantly higher than the one obtained in the previous chapter but above all increasingly far from the expected one:

$$\frac{|g_{or} - g_m|}{\sigma} = \frac{|-3.24 + 1.62|}{0{,}060} = 27.00 > 3$$

The analysis of the data variability proposed by the Origin Pro 2018 software and reported in Figure C25 highlights that the distribution of the residues is sufficiently disordered; the random error is normally distributed with the exception of the interval of residuals between +0.004 and +0.002 m, in which 5 values are included; the variance is approximately linear. It is therefore a model strongly validated by the data, but which does not prove consistent with the context of a lunar event.

Frames	T (s)	X_{ps} (m)	X_{ErrMax} (m)
0	0.000	0.000	±0.028
1	0.033	0.053	±0.028
2	0.067	0.101	±0.025
3	0.100	0.148	±0.025
4	0.133	0.195	±0.025
5	0.167	0.243	±0.025
6	0.200	0.285	±0.025
7	0.234	0.333	±0.025
8	0.267	0.374	±0.025
9	0.300	0.422	±0.025
10	0.334	-	-
11	0.367	-	-
12	0.400	0.535	±0.019
13	0.434	0.57	±0.019
14	0.467	-	-
15	0.501	-	-
16	0.534	-	-
17	0.567	0.702	±0.017
18	0.601	0.732	±0.017
19	0.634	-	-

Table C2 – "Big Muley" sequence: $X_{photoshop}$ quotas and maximum associated error

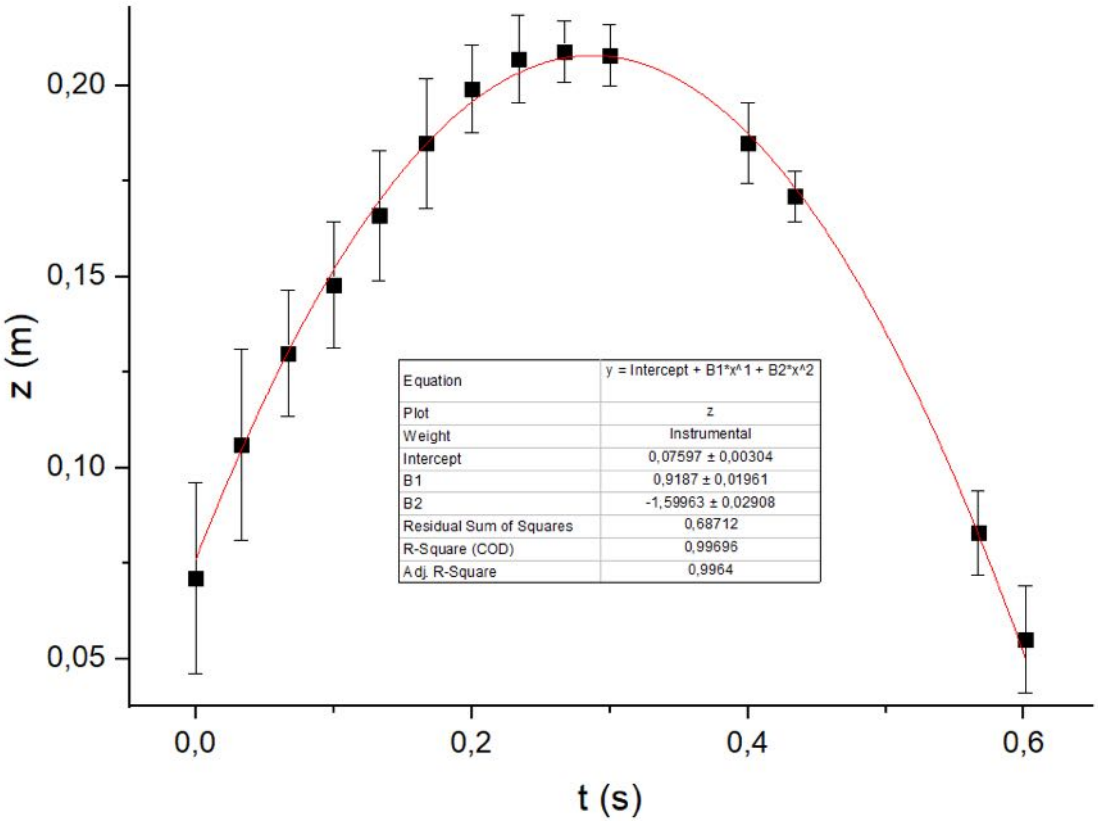

Figure C24 – Z-axis fit with maximum error range

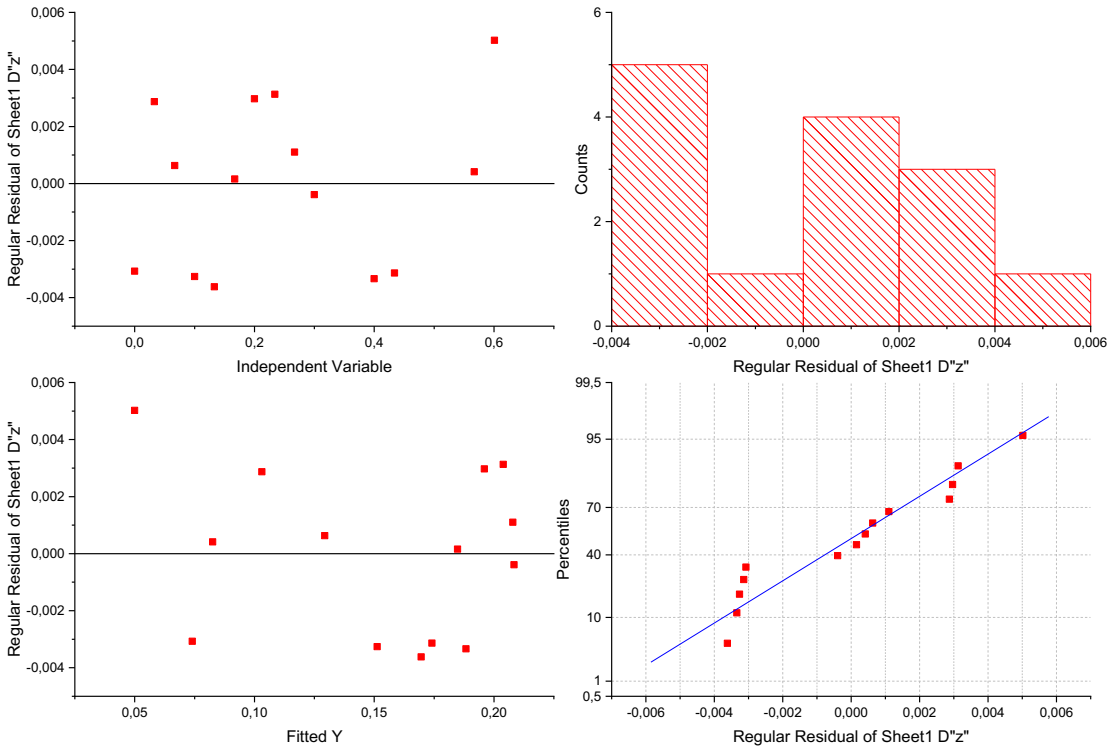

Figure C25 – Z-axis fit analysis of data variability (Origin Pro)

C.3.9 Influence of lunar surface electric fields

A possible explanation for the behavior of the dust trail on the X axis is that it was passing through an adverse electric field intense enough to cause braking.

The surface of the lunar soil is source of an electric field which is the result of various factors: the solar wind tends to make it acquire a negative charge, while UV rays trigger a photoelectric effect, giving a positive charge to the regolith and expelling a certain quantity of electrons in the area above the surface which is thus defined as "lunar plasma". If the surface is illuminated by the sun, the photoelectric effect becomes predominant over the solar wind and the surface will have a net positive charge.

Furthermore we must consider that for 25% of its revolution time around the Earth (synodic month), the Moon is located within the Earth's magnetosphere, with an important impact on the surface electric charges.

Frames	T (s)	Z_{ps} (m)	Z_{ErrMax} (m)
0	0.000	0.071	±0.019
1	0.033	0.106	±0.019
2	0.067	0.13	±0.012
3	0.100	0.148	±0.012
4	0.133	0.166	±0.012
5	0.167	0.185	±0.012
6	0.200	0.199	±0.009
7	0.234	0.207	±0.009
8	0.267	0.209	±0.008
9	0.300	0.208	±0.008
10	0.334	-	-
11	0.367	-	-
12	0.400	0.185	±0.010
13	0.434	0.171	±0.010
14	0.467	-	-
15	0.501	-	-
16	0.534	-	-
17	0.567	0.083	±0.016
18	0.601	0.055	±0.016
19	0.634	-	-

Table C3 – "Big Muley" sequence: $Z_{photoshop}$ quotas and maximum associated error

To calculate the influence of electric fields on the dust motion shot in the Big Muley sequence, we must take into account that it happened in the hour 124 of the Apollo XVI mission, the April 21st, 1972. When the event was filmed, these conditions occurred:

- The moon was outside the Earth's magnetosphere, given that the moon enters it 2-3 days before the full moon [14], and only a few hours before, the April 20th, it had just entered in the first quarter.

- The sun was inclined above the horizon line by about 25° [15] therefore a SZA = 65° occurred.

- Since we had already entered the lunar day, the lunar surface was positively charged given the prevalence of the photoelectric effect over that of the solar wind.

We can discard the implications of Tribocharges due to the rubbing of the regolith on the Moon Boot of astronaut Charles Duke, since solar wind and photoelectric effect tend to dissipate this kind of charges. The high temperatures of the lunar day can increase the mobility of the electrons further contributing to the dissipation of triboelectric charges [16].

The electric potential of the lunar surface when the sun is at Zenith (sza=0) is +10 V [17]. Since at the time of the Big Muley collection we have SZA = 66° this potential is probably less than +5 Volts, but in any case we keep the higher value.

So considering

$$E = \frac{\mathrm{V}}{d}$$

according to the literature the electric field that the lunar soil exerted on the dust particles in the sequence, about 20 cm above the ground, cannot be greater than +50 V/m.

- The potential of the lunar plasma must therefore have been around -2.5 Volts. The graph shown below (Figure C26) expresses the plasma voltage as a function of the SZA angle. [18]

Considering the Debye length of about 1 m [19], the electric field exerted by the lunar plasma on the dust particles must therefore have been about -2.5 V/m.

---

[14] https://agupubs.onlinelibrary.wiley.com/doi/full/10.1029/2019JA027401 *Unusual Location of the Geotail Magnetopause Near Lunar Orbit: A Case Study, W. S. Shang and others, Advancing Earth and Space Sciences, First published: 15 April 2020*

[15] https://www.nasa.gov/history/alsj/alsj-sunangles.html *NASA, Apollo Lunar Surface Journal 1995-2017 by Eric M. Jones, Sun Angles, Compiled by Brian W. Lawrence. Last revised 11.10.2005.*

[16] https://ntrs.nasa.gov/api/citations/20160013625/downloads/20160013625.pdf *The Electrostatic Environments of the Moon […] NASA, Kennedy Space Center, Carlos I. Calle, Ph.D. October 27th, 2016*

[17] https://iopscience.iop.org/article/10.1088/1674-4527/19/6/77 *IOP Science, Lunar surface potential and electric field, Lei Li and others 2019*

[18] https://iopscience.iop.org/article/10.1088/1674-4527/19/6/77 *IOP Science, Lunar surface potential and electric field, Lei Li and others 2019*

[19] https://www.lpi.usra.edu/meetings/lpsc2010/pdf/2406.pdf *Characterization of a UV - generated photoelectron sheath. A. Dove, 41st Lunar and Planetary Science Conference (2010)*

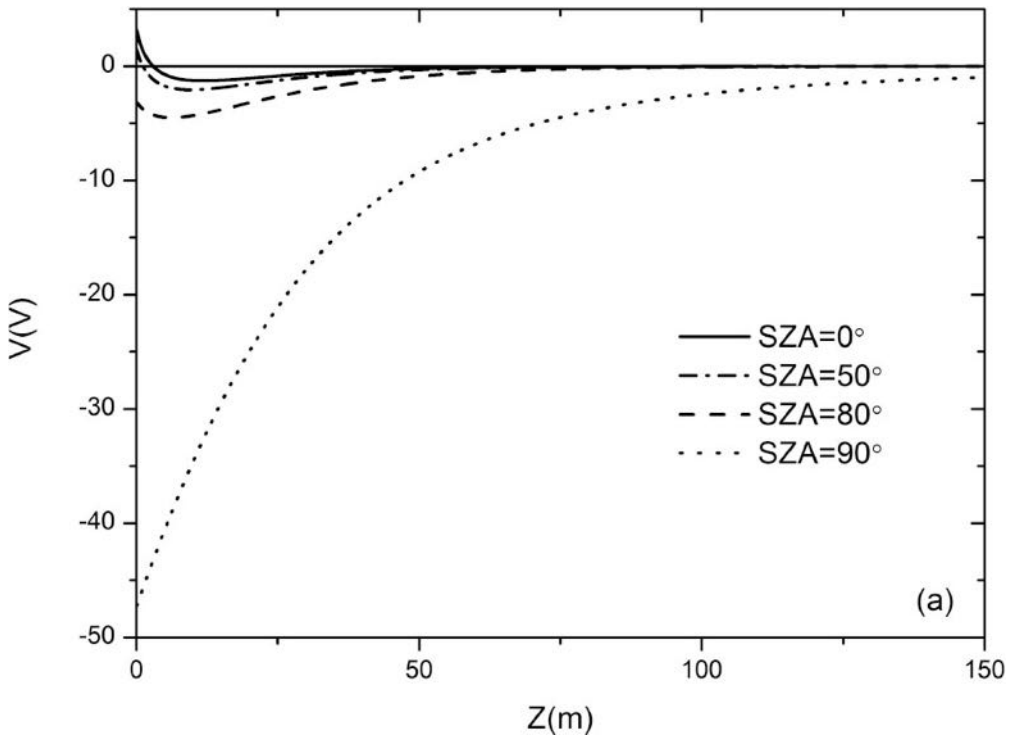

Figure C26 - Sheath potential profiles from the subsolar (sza = 0°) to the terminator on the dayside for sza = 0°, 50°, 80° and 90°.

- Lunar dust is a poorly conductive material, it maintains its electrostatic charge locally. [20] The fact that dust is raised from the ground by an area of the surface on which the astronaut projects his shadow for a few seconds cannot have any impact on the charge of the particle.

Since we are tracing the motion of the dust trail over a completely flat and smooth area, the first consideration we can make is that the vertically oriented electric fields should not have had an influence on the horizontal component of the motion. The impact of a vertically oriented electric field on the particle motion could never produce a track asymmetric with respect to the vertical axis like the one detected (Figure C27).

The second consideration, is that given the intensities of the electric fields involved and the average dimensions - and therefore the average charge - of the particles raised by the astronaut's kick, the resulting electric field would have had an effect on the motion of the particles completely negligible also on Z axis.

Electric Field $E = V / d$

Electric Force $Fe = qE$

Particle charge $Q = 4\pi\epsilon_0 rU$

Acceleration imparted by the electric force $a_e = Fe / m$

[20] https://agupubs.onlinelibrary.wiley.com/doi/10.1029/2008GL034785 *Concerning the dissipation of electrically charged objects in the shadowed lunar polar regions, W.M. Farrell and others, Advancing Earth and Space Sciences, First published: 04 October 2008*

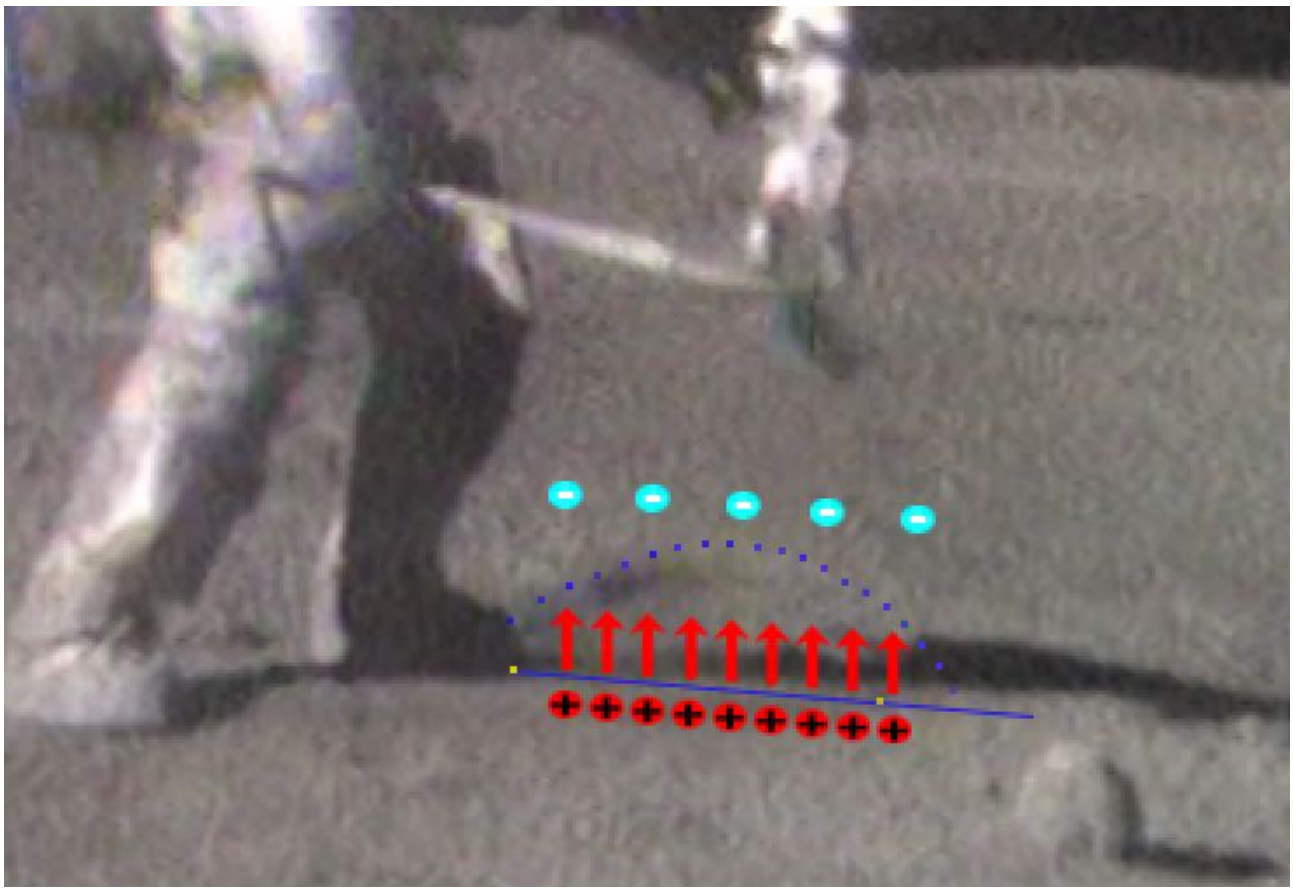

Figure C27 - Direction of the overall electric field (surface - lunar plasma) crossed by the dust trail.

Max lunar surface potential: +10 Volt

Particle radius: 95×10^{-6} m

Average mass of the particle: $1{,}06 \times 10^{-8}$ Kg

$E_{soil(min)} = 10 / 0{,}20 = 47{,}62$ V/m

$E_{soil(max)} = 10 / 0{,}02 = 500$ V/m

$E_{plasma} = -2{,}5/1 = -2{,}5$ V/m (Debye length = 1 m)

$E_{total(min)} = 50{,}12$ V/m

$E_{total(max)} = 502{,}5$ V/m

$Q = 4\pi \times 8.85 \times 10^{-12} \times 95 \times 10^{-6} \times 10 = 1{,}056 * 10^{-13}$ C

$Fe_{(min)} = 1{,}056 * 10^{-13} \times 50{,}12 = 5{,}29 * 10^{-12}$

$Fe_{(max)} = 1{,}056 * 10^{-13} \times 502{,}5 = 5{,}31 * 10^{-11}$

$a_{e(min)} = 5{,}29 * 10^{-12} / 1{,}06 \times 10^{-8} = 5{,}61 \times 10^{-4}$ m/s2

$a_{e(max)} = 5{,}31 * 10^{-11} / 1{,}06 \times 10^{-8} = 5{,}63 \times 10^{-3}$ m/s2

Considering the official framerate the particle would reach the vertex of the parabola with the frame number 9 when t = 0,300 s, so the increase of maximum quota reached thanks to a_e would be:

$S_{(min)} = 5{,}61 \times 10^{-4} \times 0{,}3^{\,2} = 5{,}05 \times 10^{-5}$ m

$S_{(max)} = 5{,}63 \times 10^{-3} \times 0{,}3^{\,2} = 5{,}10 \times 10^{-4}$ m

C.3.10 Hypothesis of motion with air resistance.

In an attempt to identify a better model, the data collected are proposed for a new fit, this time also on the X-Axis according to a non-linear equation [*Ann. C10*]. To introduce this choice, we must clarify some basic assumptions.

Getting inspiration once again from the study "Ballistic motion of dust particles in the Lunar Roving Vehicle dust trails" by Mihaly Horanyi and Hsiang-Wen Hsu, and in particular from the section "IV. Discussion", a motion model with air resistance is adopted on the X-axis.

Abandoning the model that saw dust particles reduced to a material point, let's consider a braking action originating from the viscous resistance of the air, which, given the relatively low speed (Reynolds number Re < 1), prevails over the pressure resistance. [21]

The equations representing the motion will be [22] :

$E_5)\ X_{airdrag}(t) = X_0 + V_{x0} * \tau * (1 - e^{\frac{-t}{\tau}})$

$E_6)\ Z_{airdrag}(t) = Z_0 + (V_{z0} + (g * \tau)) * \tau * (1 - e^{\frac{-t}{\tau}}) - (g * \tau) * t$

where $\tau = \frac{m}{\beta * d}$ is the time which horizontal velocity takes to reach $\frac{1}{e}$ of its initial value.

Figures C28 – C29 – C30 represent the results of the fit of the data collected on the X-axis with equation E_5

As can be seen from Figure C30 on the X axis, the model with air resistance proves to be more effective than the linear one. The time τ which in the software analysis is indicated with the parameter h, is identified by the fit with the approximate value of 1.1 seconds (Figure C29).

---

[21] *Fundamentals of Physics and Chemistry of the Atmosphere*
Guido Visconti, Copyright Springer Science & Business Media, 2001.

[22] *https://www.researchgate.net/publication/258468670 - M. Horanyi e Hsiang-Wen Hsu, "Ballistic motion of dust particles in the Lunar Roving Vehicle dust trails", American Journal of Physics, 2012*

Equation	X = o + v*h*(1 - exp(-t/h))
Report Status	New Analysis Report
Special Input Handling	
Data Filter	No

Input Data

Parameters

		Value	Standard Error	t-Value	Prob>|t|	Dependency
x	o	-0,00284	0,00227	-1,24784	0,238	0,88304
	v	1,60332	0,0198	80,98291	2,22045E-16	0,98263
	h	1,06571	0,04587	23,23091	1,06616E-10	0,96883

Reduced Chi-sqr = 0,0168025549216
COD(R^2) = 0,99988173703936
Iterations Performed = 6
Total Iterations in Session = 6
Fit converged. Chi-Sqr tolerance value of 1E-9 was reached.
Standard Error was scaled with square root of reduced Chi-Sqr.
Some input data points are missing.

Statistics

	x
Number of Points	14
Degrees of Freedom	11
Reduced Chi-Sqr	0,0168
Residual Sum of Squares	0,18483
R-Square (COD)	0,99988
Adj. R-Square	0,99986
Fit Status	Succeeded(100)

Fit Status Code :
100 : Fit converged. Chi-Sqr tolerance value of 1E-9 was reached.

Summary

	o		v		h		Statistics	
	Value	Standard Error	Value	Standard Error	Value	Standard Error	Reduced Chi-Sqr	Adj. R-Square
x	-0,00284	0,00227	1,60332	0,0198	1,06571	0,04587	0,0168	0,99986

ANOVA

		DF	Sum of Squares	Mean Square	F Value	Prob>F
x	Regression	3	6278,33635	2092,77878	124551,22413	0
	Residual	11	0,18483	0,0168		
	Uncorrected Total	14	6278,52118			
	Corrected Total	13	1562,85707			

At the 0.05 level, the fitting function is significantly better than the function X=constant.

Figure C28 – X-axis, non-linear fit: parameters obtained and their reliability

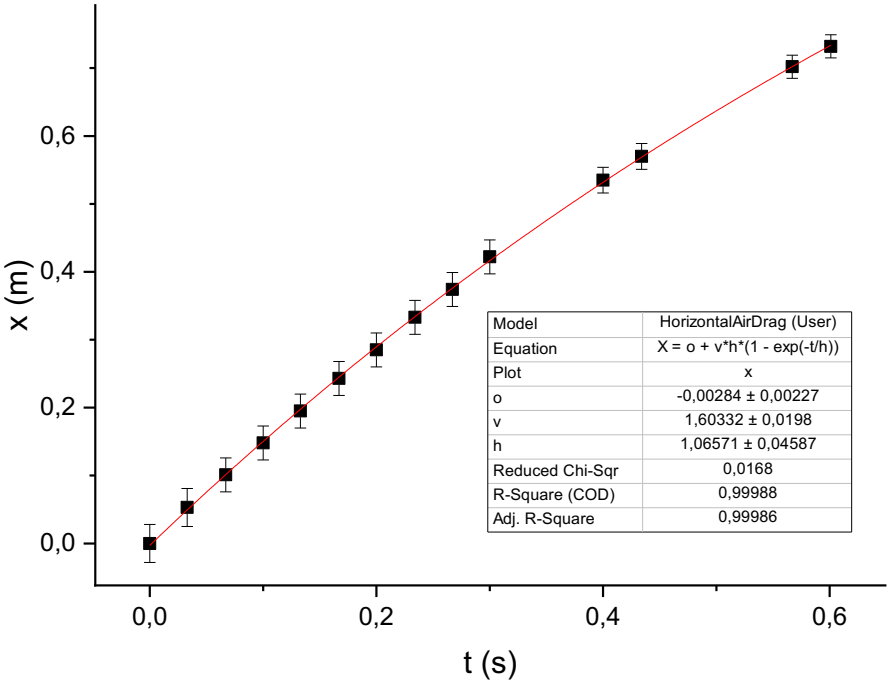

Figure C29 – X-axis, motion plot with air resistance

Description

	Model1	Model2
Input Data	[Book1]Sheet1!(B"t",C"x",E1"Xerr")	[Book1]Sheet1!(B"t",C"x",E1"Xerr")
Fit Report	[Book1]FitLinear1	[Book1]FitNL1
Equation	y = a + b*x	X = o + v*h*(1 - exp(-t/h))
Function		HorizontalAirDrag (User)
Number of Points	14	14
Number of Parameters	1	3

Preferred Model

	Model Name
AIC	Model2
BIC	Model2
F-Test	Model2

Akaike's Information Criterion Test (AIC)

	RSS	N	Params	AIC	Akaike Weight
Model1	5,84112	14	1	-7,14698	1,25517E-9
Model2	0,18483	14	3	-48,13896	1

Model2 has lower AIC value and so is more likely to be correct.
This model is 7.96704e+008 times more likely to be correct.

Bayesian Information Criterion Test (BIC)

	RSS	N	Params	BIC	Diff BIC
Model1	5,84112	14	1	-6,95977	43,06741
Model2	0,18483	14	3	-50,02718	0

Model2 has lower BIC value and so is more likely to be correct.
BIC difference greater than 10 gives decisive conclusion that Model2 is correct.

F-test

	F	Numer.DF	Denom.DF	Prob > F
	168,31643	2	11	5,64281E-9

At the 0.05 significance level, Model2 is more likely to be correct.
Note: The F-test results assume the two models are nested.

Figure C30 – X-axis: comparison between linear model and model with air resistance

To verify the consistency of this data we refer to the mechanical characteristics of the dust particles starting from those of the simulant of the lunar regolith used. Apollo program engineers and geologists developed 5 lunar soil simulants (LSS). In 1970 in Dayton, Ohio, the LSS-4 simulant was used in a series of mechanical tests on the wheels of the Lunar Rover because researchers considered it to be particularly suitable for representing the characteristics of the lunar soil for the Apollo 15 mission. [23]

About Apollo 16 it was then ascertained that the soil characteristics of the stations visited during the EVAs did not differ from those of previous missions. Figure C29 shows the comparison of the grain size distribution of the lunar soil in the lunar landing areas chosen for the various missions. [24]

[23] https://www.lpi.usra.edu/lunar/documents/NASA%20CR-121075.pdf *A Study and Analysis of the MSFC Lunar Roving Vehicle Dust Profile Test Program by C. Howell Mullis, November, 1971 - College Of Engineering University Of Alabama [Ann. B8]*

[24] https://www.nasa.gov/wp-content/uploads/static/history/alsj/a16/as16psr.pdf *Apollo 16, Preliminary Science Report, NASA 25 May 1973 (pag 8.5)*

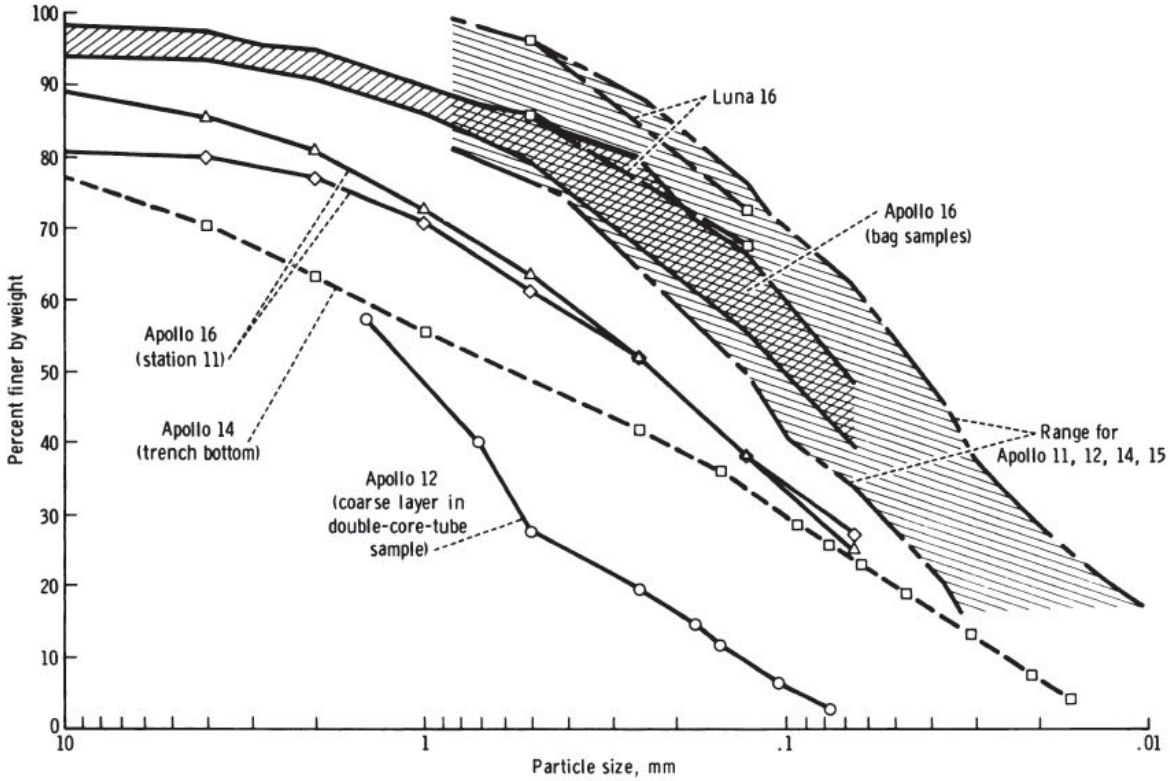

Figure C31 - Comparison of the grain size distribution of lunar soil in the Apollo missions

As can be seen from the graph, the distribution found in the Apollo 16 mission constitutes a subset of the distribution range relating to the previous missions. It is therefore plausible that the LSS-4 simulant was also used in relation to Apollo 16, or at least it was considered eligible to replicate the characteristics of the lunar soil for the Descartes Highlands and the Plum Crater. Below are its mechanical characteristics [24]:

LSS-4
Official Name: Lunar Soil Simulant 4
Parent Rock Source: Basalt Rock Company, Napa, California
Material: Crushed Basalt

Grain Size Distribution:
D60 = 0.19 mm
D10 = 0.0065 mm
Cu (Uniformity coefficient) D60/D10 = 29.3
Distribution Classification: Well-Graded
Color: Cement Gray
Manufacturer and Test Laboratory:
U.S. Corps of Engineers Waterways Experiment Station, Vicksburg, Mississippi

Once the physical characteristics of the simulant are known and their compatibility with those of the lunar soil is verified, we proceed with the construction of the mechanical model of dust particles, approximating it to a sphere in order to identify the best value of τ indicated by the Origin Pro software in the fit model with air resistance. With the help of the spreadsheet [*Ann. C7*], the results obtained are the following:

Particle Diameter	344	μm
Surface of Particle Section	0.093	mm^2
Particle Volume	$2.13144*10^{-11}$	m^3
Basalt Density	2950	Kg/m^3
Particle Mass	$6.28776*10^{-8}$	Kg
Viscosity Air Coefficient	$1.81000*10^{-5}$	
Constant Sphere resistance	9.42478	
β	$1.70588*10^{-4}$	
τ	1.07149	s

Table C4 – Mechanical data characteristic of the dust particles

To obtain τ = 1.07 s it is therefore necessary to assume that the particles had a diameter of 344 microns. This is a value that can be considered consistent with the scientific data available, relating to the simulant used for the tests and to the lunar soil in question. This grain size value is positioned in the graph in Figure C31 as indicated in the following figure C32.

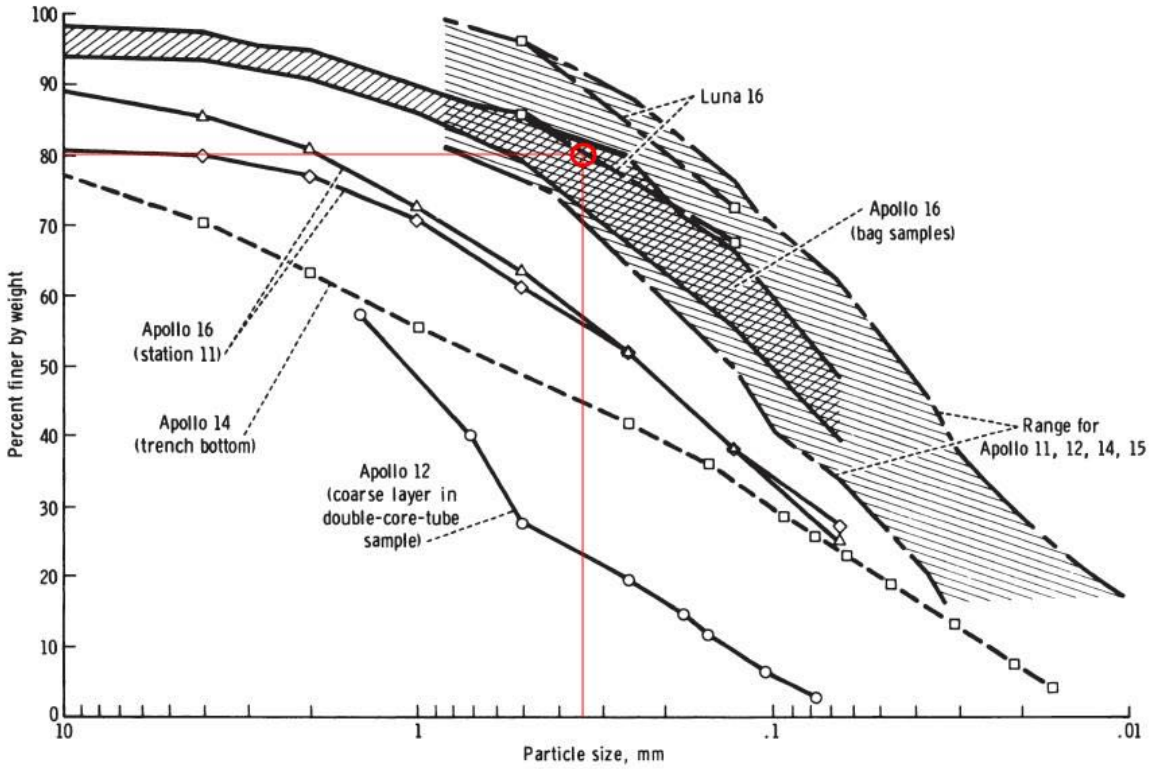

Figure C32 – Consistency of the particle size result

In fact, according to the scientific information available, approximately 20% of the particulate in question (present on the lunar soil or simulated in the laboratory) had a diameter equal to or greater than that taken into consideration for the model. And then it is legitimate to determine a higher-than-average value, since we are tracing the head of the dust spurt: the biggest particles tend to be less subject to the braking action of the air and therefore to have a longer trail.

We, therefore, perform the fit of the data collected on the Z-Axis by setting τ' = 1.07 s as the fixed parameter of the E6 equation and we observe that the fit is excellent also in this case (Figures C33, C34, and C35).

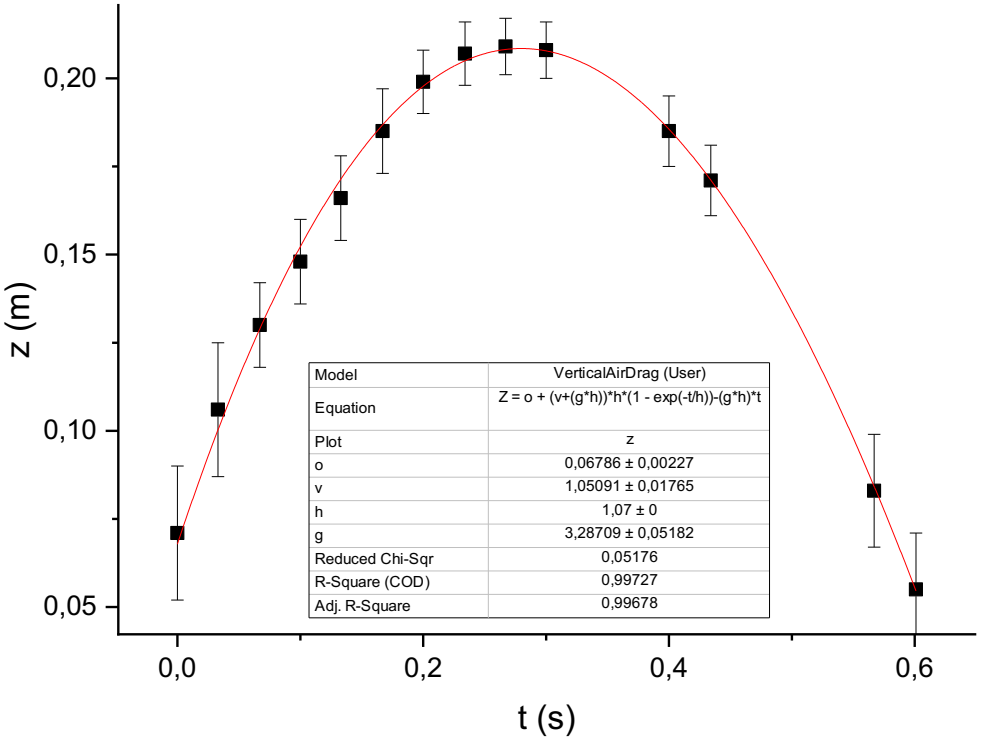

Figure C33 - Plot of data collected from tracing on the Z-axis with fit equation E_6

Equation	Z = o + (v+(g*h))*h*(1 - exp(-t/h))-(g*h)*t
Report Status	New Analysis Report
Special Input Handling	
Data Filter	No

Input Data

Parameters

		Value	Standard Error	t-Value	Prob>|t|	Dependency
z	o	0,06786	0,00227	29,87432	6,97842E-12	0,91431
	v	1,05091	0,01765	59,55704	3,77476E-15	0,97703
	h	1,07	0	--	--	0
	g	3,28709	0,05182	63,43127	1,77636E-15	0,94284

Reduced Chi-sqr = 0,051761378751
COD(R^2) = 0,997273567069 84
Iterations Performed = 4
Total Iterations in Session = 4
Fit converged. Chi-Sqr tolerance value of 1E-9 was reached.
Some parameter values were fixed.
Standard Error was scaled with square root of reduced Chi-Sqr.
Some input data points are missing.

Statistics

	z
Number of Points	14
Degrees of Freedom	11
Reduced Chi-Sqr	0,05176
Residual Sum of Squares	0,56938
R-Square (COD)	0,99727
Adj. R-Square	0,99678
Fit Status	Succeeded(100)

Fit Status Code :
100 : Fit converged. Chi-Sqr tolerance value of 1E-9 was reached.

Summary

	o		v		h		g		Statistics	
	Value	Standard Error	Value	Standard Error	Value	Standard Error	Value	Standard Error	Reduced Chi-Sqr	Adj. R-Square
z	0,06786	0,00227	1,05091	0,01765	1,07	0	3,28709	0,05182	0,05176	0,99678

ANOVA

		DF	Sum of Squares	Mean Square	F Value	Prob>F
z	Regression	3	3792,82963	1264,27654	24425,09405	0
	Residual	11	0,56938	0,05176		
	Uncorrected Total	14	3793,39901			
	Corrected Total	13	208,8352			

At the 0.05 level, the fitting function is significantly better than the function Z=constant.

Figure C34 - Fit values, data relating to the Z-Axis with fit equation E_6

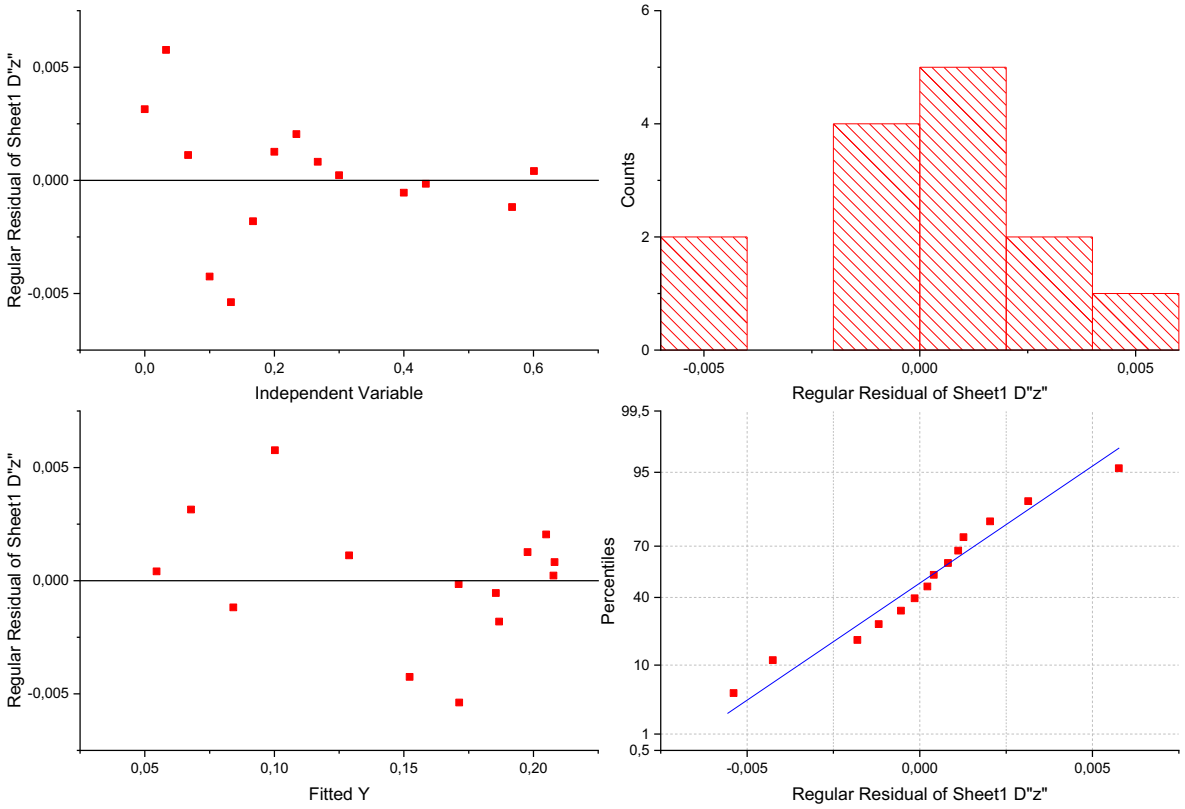

Figure C35 – Analysis of residuals, fit of data relating to the Z-Axis with fit equation E_6

C.4.1 Framerate Correction

By applying what has already been used in B.3.4.2 we can calculate an appropriate framerate correction factor so as to be able to bring *g* back to the expected values:

$Z(t) = Z_0 + (V_{z0} + (g * \tau)) * \tau * (1 - e^{\frac{-t}{\tau}}) - (g * \tau) * t$ is equivalent to

$Z'(t) = Z_0 + (V'_{z0} + (g' * \tau')) * \tau' * (1 - e^{\frac{-t'}{\tau'}}) - (g' * \tau') * t'$ when

$$t' = \frac{t}{\alpha}; \quad \tau' = \frac{\tau}{\alpha}; \quad v'_{z0} = \alpha \cdot v_{z0} \quad \text{e} \quad g'_{av} = g_{av} \cdot \alpha^2$$

Considering that in the fit carried out, the results are consistent only with the models with air resistance, the correction factor is calculated considering the value of terrestrial g = 9.81 m/s2:

$\alpha = \sqrt{\frac{9.81}{3.29}} = 1.73$ in this case, therefore, the correct shooting framerate is 51.75 fps, and the time τ' takes on the value of 0.62 seconds, obtainable with particles of at least 262 microns diameter, a value that is fully admissible in the studied context.

Even approximating the framerate to the more plausible value of 50 fps, the fit [*Ann. C11*] performed according to E_6 with fixed parameters g = 9.81 m/s^2 and τ' = 0.62 s always proves to be excellently effective on both axes (Figures C36 and C37).

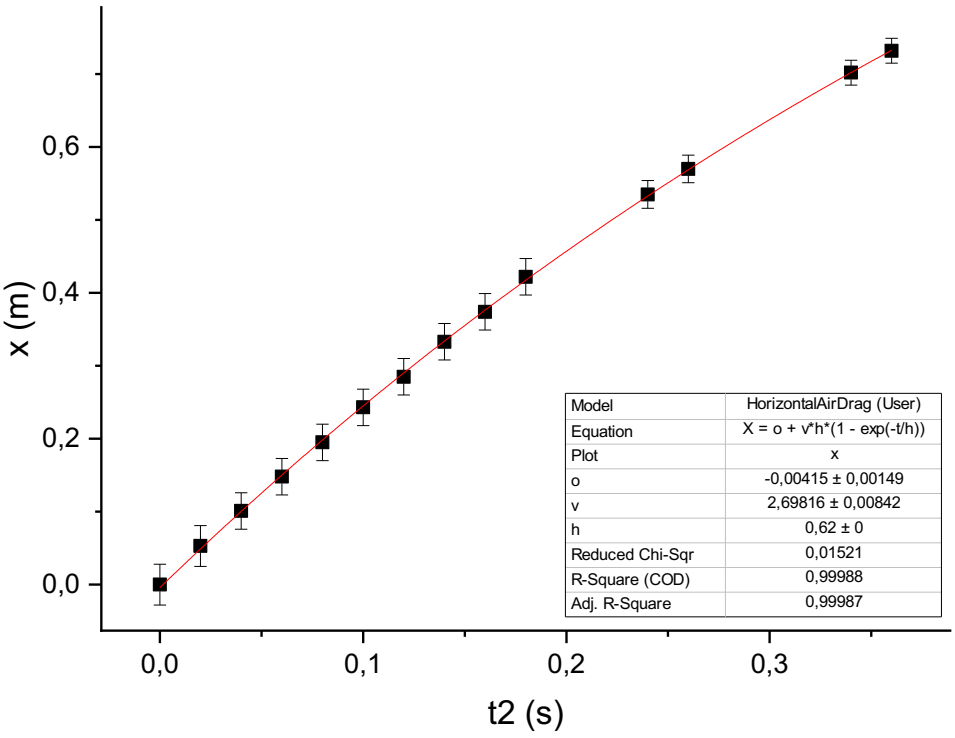

Equation	X = o + v*h*(1 - exp(-t/h))
Report Status	New Analysis Report
Special Input Handling	
Data Filter	No

Input Data

Parameters

		Value	Standard Error	t-Value	Prob>|t|	Dependency
x	o	-0,00415	0,00149	-2,77664	0,01675	0,75483
	v	2,69816	0,00842	320,51365	0	0,75483
	h	0,62	0	--	--	0

Reduced Chi-sqr = 0,0152116199123
COD(R^2) = 0,99988320145043
Iterations Performed = 4
Total Iterations in Session = 4
Fit converged. Chi-Sqr tolerance value of 1E-9 was reached.
Some parameter values were fixed.
Standard Error was scaled with square root of reduced Chi-Sqr.
Some input data points are missing.

Statistics

	x
Number of Points	14
Degrees of Freedom	12
Reduced Chi-Sqr	0,01521
Residual Sum of Squares	0,18254
R-Square (COD)	0,99988
Adj. R-Square	0,99987
Fit Status	Succeeded(100)

Fit Status Code :
100 : Fit converged. Chi-Sqr tolerance value of 1E-9 was reached.

Summary

	o		v		h		Statistics	
	Value	Standard Error	Value	Standard Error	Value	Standard Error	Reduced Chi-Sqr	Adj. R-Square
x	-0,00415	0,00149	2,69816	0,00842	0,62	0	0,01521	0,99987

ANOVA

		DF	Sum of Squares	Mean Square	F Value	Prob>F
x	Regression	2	6278,33864	3139,16932	206366,5368	0
	Residual	12	0,18254	0,01521		
	Uncorrected Total	14	6278,52118			
	Corrected Total	13	1562,85707			

At the 0.05 level, the fitting function is significantly better than the function X=constant.

Figure C36 - Plot and data related to the X-Axis with E5 fit equation and framerate of 50 fps

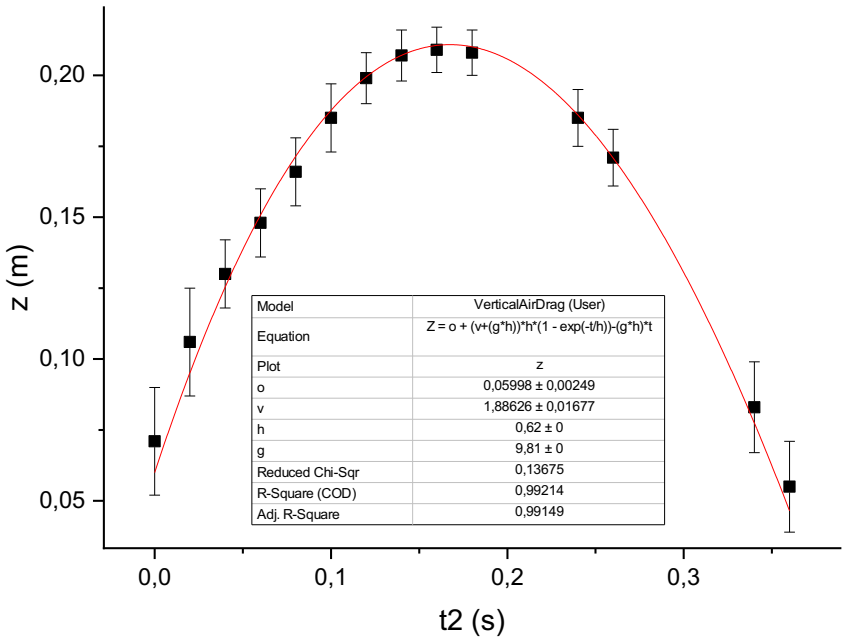

Equation	Z = o + (v+(g*h))*h*(1 - exp(-t/h))-(g*h)*t
Report Status	New Analysis Report
Special Input Handling	
Data Filter	No

Input Data

Parameters

		Value	Standard Error	t-Value	Prob>|t|	Dependency
z	o	0,05998	0,00249	24,12911	1,54359E-11	0,81096
	v	1,88626	0,01677	112,45925	0	0,81096
	h	0,62	0	--	--	0
	g	9,81	0	--	--	0

Reduced Chi-sqr = 0,136753433472
COD(R^2) = 0,99214193200573
Iterations Performed = 4
Total Iterations in Session = 4
Fit converged. Chi-Sqr tolerance value of 1E-9 was reached.
Some parameter values were fixed.
Standard Error was scaled with square root of reduced Chi-Sqr.
Some input data points are missing.

Statistics

	z
Number of Points	14
Degrees of Freedom	12
Reduced Chi-Sqr	0,13675
Residual Sum of Squares	1,64104
R-Square (COD)	0,99214
Adj. R-Square	0,99149
Fit Status	Succeeded(100)

Fit Status Code :
100 : Fit converged. Chi-Sqr tolerance value of 1E-9 was reached.

Summary

	o		v		h		g		Statistics	
	Value	Standard Error	Value	Standard Error	Value	Standard Error	Value	Standard Error	Reduced Chi-Sqr	Adj. R-Square
z	0,05998	0,00249	1,88626	0,01677	0,62	0	9,81	0	0,13675	0,99149

ANOVA

		DF	Sum of Squares	Mean Square	F Value	Prob>F
z	Regression	2	3791,75797	1895,87898	13863,48361	0
	Residual	12	1,64104	0,13675		
	Uncorrected Total	14	3793,39901			
	Corrected Total	13	208,8352			

At the 0.05 level, the fitting function is significantly better than the function Z=constant.

Figure C37 - Plot and data related to the Z-Axis with E6 fit equation and framerate of 50 fps

The theoretical model so obtained, relating to a terrestrial parabolic motion of basalt particles in the presence of viscous friction caused by air, finds substantial identity with the experimental results for granulometric values of the dust compatible with those of the simulants used in technical tests conducted for the preparation of Apollo missions, if we accept that the camera recording framerate was 50 fps instead of 29.97 fps.

About the Authors

Alessio Michelotti (ORCID iD: https://orcid.org/0000-0002-3822-104X)
was born in Lucca (IT) the 31-08-72, and obtained a scientific high school diploma at the Liceo Lorenzini in Pescia in 1991 with a specialization in Physics - Mathematics.
He is a professional researcher in the field of Culture with different publications edited by academic publishers in Italy (like Bulzoni Editore and CUEM).

PhD Andrea Simon (ORCID iD: https://orcid.org/0009-0001-3971-4305)
Headmaster in the "Novalis" Italian Waldorf High School where he is also mathematics and physics teacher, he obtained his Master's Degree in Physics and his teaching qualification from the University of Padua. Among the most significant previous published works is "*First Results of a Scintillating GEM Detector for 2-D Dosimetry in an Alpha Beam*" edited by IEEE in 2008.

Authors contribution

- Alessio Michelotti: Conceptualization, Data curation, Investigation, Project administration, Visualization, Writing – original draft
- Andrea Simon: Conceptualization, Formal Analysis, Methodology, Software, Supervision, Validation

Conflict of interests

The authors declare that there are no conflicts of interest.

ACKNOWLEDGMENTS

Many people, directly and indirectly, have made this study possible through their collaboration. Most of them have not had the opportunity to see the full content of this work, which may be partly outside their respective research fields. Furthermore, the final results of this paper may not reflect, or be in contradiction with, their beliefs or research. However, we would like to thank each of them for their help and for the effectiveness of their valuable contribution.

We would like to thank for their methodological suggestions and encouragement in research: prof. Luis Bilbao, Universidad de Buenos Aires - Departamento de Física; prof. Andrea Simon, Scuola Superiore Novalis, San Vendemiano (Treviso, Italy); prof. Pasquale Bosso, University of Lethbridge (Canada); prof. Derek Bolton, University of Oxford (United Kingdom); Prof. Franco Macchini, University of Pisa (Italy).

This study would not have been possible without the technical information, scientific support and documentary materials provided by:

- James T. Hawes, IT Expert technical, writer & editor
- Mark Gray, Spacecraft Films (Atlanta GA), NASA contractor for Video Editing
- Russ Andersson, SynthEyes, Andersson Technologies LLC (Phoenixville, PA)
- Douglas Brown, Open Source Physics (OSP), Davidson College, Davidson NC, USA

This study has been reviewed by the following researchers:

- **Andreas Märki**, Zurich (CH); Master of Engineering, Swiss Aerospace Industry Technician. Revised sections: Preamble; Sections A, B, C, D.

- Andrea Simon, Vittorio Veneto (IT); Physics teacher and headmaster at Scuola Superiore "Novalis", San Vendemiano (Treviso, IT)**.** Revised sections: Preamble; Sections A, B, C, E.

- **Luis Bilbao**, Buenos Aires (ARG); PhD at the Physics University of Buenos Aires; more than 100 publications in international journals; reviewer for the American Journal of Physics and other major scientific journals. Revised sections: Sections B, E.

- **Dwight Steven-Boniecki**, Köln (DE); Author of Space History: NASA Skylab and Soyuz Mission Reports Editor/Compiler. Revised sections: Preamble; Section A.

- David Chandler, Denver, Colorado (USA); Teacher at Porterville College, Porterville, CA / Physics, Mathematics, and Engineering; publications in American Journal of Physics and other Journals. Served on "The Physics Teacher" Editorial Board as a reviewer.
Revised sections: Preamble.

- **Francesco Vinci**, Avola (IT); Order of Architects P.P.C. Siracusa province; Teacher at Università degli Studi di Catania, Facoltà di Scienze dell'Architettura e dell'Ingegneria Edile. Creator of "Brunelleschi" software for prospective restitution. Revised sections: Preamble; Section A.

Their contribution to the review process is documented in the specific appendix (not attached here).

The previous study "**Analytical Methods for Tracking Bodies Motions on the Lunar Surface in Apollo XVI Footage – *An analysis method*"** has been reviewed as Preprint on the **qeios.com** platform the 22nd April 2024: https://www.qeios.com/read/IA8MXE

The following researchers further revised that work:

Dr. **Jens Biele German** (h-index 36) Aerospace Center (DLR), Köln (DE) – Astronomy, Geophysics, Experimental Physics and Thermodynamics Researcher. Revised sections: Sections A, B, C.

Dr. **Alexey Artamonov** (h-index 9), National Research Nuclear University MEPhI - Moscow Engineering Physics Institute, Moscow (RU). Revised sections: Sections A, B, C.

(English translation by Roberto Leopardi)